NATIONAL ADVISORY COMMITTEE FOR AERONAUTICS

TECHNICAL NOTE 3149

PREDICTION OF LOSSES INDUCED BY ANGLE OF ATTACK IN CASCADES OF SHARP-NOSED BLADES FOR INCOMPRESSIBLE AND SUBSONIC COMPRESSIBLE FLOW

By James J. Kramer and John D. Stanitz

Lewis Flight Propulsion Laboratory
Cleveland, Ohio

Washington
January 1955

NATIONAL ADVISORY COMMITTEE FOR AERONAUTICS

TECHNICAL NOTE 3149

PREDICTION OF LOSSES INDUCED BY ANGLE OF ATTACK IN CASCADES OF SHARP-NOSED BLADES FOR INCOMPRESSIBLE AND SUBSONIC COMPRESSIBLE FLOW

By James J. Kramer and John D. Stanitz

SUMMARY

A method of computing the losses in total pressure caused by a non-zero angle of attack at the inlet to a row of sharp-nosed blades is developed for both incompressible and subsonic compressible flow. The method is based on momentum considerations across a row of zero-thickness flat plates and assumes that the blade force is normal to the plate surface. The results of the analysis are presented in a series of figures showing the variation of the total-pressure loss coefficient and the static-pressure coefficient with upstream flow angle and angle of attack for incompressible flow and with upstream flow angle, angle of attack, and upstream Mach number for compressible flow. The figures indicate for the range of variables considered that increases in upstream flow angle cause sharp rises in total-pressure loss coefficient and corresponding drops in static-pressure coefficient for negative angles of attack, but for positive angles of attack and upstream flow angles less than 60° there is little variation in total-pressure loss coefficient with upstream flow angle. Also, increases in upstream Mach number cause only slightly higher values of total-pressure loss coefficient for positive angles of attack. A maximum value of static-pressure coefficient occurs for a given value of upstream flow angle at a certain positive angle of attack, beyond which further increases in angle of attack result in decreases in static-pressure coefficient. The angle of attack at which this maximum static-pressure coefficient occurs decreases as the upstream Mach number increases.

CT-1

INTRODUCTION

When a fluid enters a compressor or turbine cascade of sharp-nosed blades at an angle different from that of the blade camber line at the nose, potential-flow solutions indicate an acceleration to an infinite velocity by the fluid as it moves from the stagnation point around the

sharp nose (ref. 1, pp. 122-124, for example). Real fluids cannot overcome the resultant steep pressure gradient so that the flow separates off the suction surface of the blade at the sharp nose. The separation and subsequent mixing losses caused by the nonzero angle of attack, that is, the angle between the relative flow direction far upstream of the blade row and the tangent to the blade camber line at the nose, constitute a major source of loss in the internal flow of centrifugal and axial-flow compressors. This is indicated by the detailed experimental data of reference 2 for a centrifugal compressor.

A simple method of predicting the magnitude of these losses for incompressible flow only is presented in reference 3 (pp. 129 and 150) and will be discussed herein. In reference 4 (p. 182), the losses are correlated with the kinetic energy of the fluid associated with the upstream velocity component normal to the blade surface. The method is dependent upon experimental data for the value of the correlation coefficients, and, hence, these values are influenced by other factors such as blade-end effects. In reference 5, the inlet loss is assumed to be equal to the kinetic energy of the fluid associated with the upstream velocity component normal to the blade surface. Good agreement with experimental results of turbine performance was obtained. However, the results of the analysis reported herein are not applicable to any row of blunt leading-edge blades.

A simple method based on momentum considerations across an infinite cascade of flat plates was therefore developed at the NACA Lewis laboratory. This method will predict the maximum total-pressure losses caused by nonzero angle of attack at the inlet to a row of sharp-nosed blades. The analysis was carried out for both incompressible and subsonic compressible nonviscous flow. The results are presented in a series of figures showing the variations in total-pressure loss coefficient and static-pressure coefficient with angle of attack and upstream flow direction for incompressible flow and with angle of attack, upstream flow direction, and upstream Mach number for compressible flow.

METHOD OF ANALYSIS

Preliminary Considerations

The first potential-flow solution for flow past an isolated zero-thickness flat plate was similar to that shown in figure 1(a) (see ref. 6). This so-called Dirichlet flow was symmetrical and indicated zero lift and drag. Physically unrealistic infinite velocities were indicated for both the nose and tail sections. The flow was more accurately described when the Joukowski condition was specified for the tail section (fig. 1(b)). The addition of this condition eliminated the infinite velocity at the tail and resulted in a lift force, normal to the undisturbed-flow direction, but the drag remained zero. Also, in this

Joukowski flow the velocity at the nose remained infinite. (This infinite velocity gives rise to a "suction force" that results from the hypothetical, infinite, negative pressure acting over the zero area of the nose. This suction force cancels the drag force that would otherwise exist as a result of the finite pressures acting normal to the plate.) The next attempt to describe the flow was by the free-streamline, or cavity-flow, method of Kirchhoff and Helmholtz (refs. 7 and 8). This method avoids infinite velocities at the nose by assuming separated flow at that point (fig. 1(c)). For this solution the suction force is zero; the resultant force, now due to finite pressures only, is normal to the plates so that a drag force, parallel to the undisturbed-flow direction, exists (fig. 1(c)). (In the free-streamline solution for a flat plate at an angle of attack, the size of the separated region is much larger than that which is found experimentally, so that the drag forces indicated by the theory are excessive.)

The method used in this report approximates the cascade of arbitrary sharp-nosed blades by a cascade of zero-thickness flat plates and assumes that the flow separates at the nose, with the result that infinite velocities are avoided at the leading edge. Therefore, the resultant force on the plate is caused by finite pressures only, and this force is perpendicular to the plate since skin friction is assumed to be zero. These assumptions together with momentum and continuity considerations determine the inlet loss.

Physically, the results of the analysis presented herein can be interpreted in two ways. First, this analysis yields the losses in total pressure, exclusive of those associated with skin friction, caused by nonzero angle of attack in a cascade of zero-thickness flat plates. Stalling of the plates does not alter the validity of the equations derived herein. In this analysis the effect of stall is reflected in the magnitude of the exit deviation angle, that is, the angle between the downstream flow direction and the blade direction. The numerical results obtained assuming zero deviation angle would apply for cascades of high solidity or small angles of attack or both. The effects of deviation angle are discussed after the development of the equations for the total- and static-pressure changes across the blade row.

Secondly, the analysis can be interpreted as indicating the trends in losses caused by nonzero angle of attack in a cascade of arbitrary sharp-nosed blades. The loss induced by nonzero angle of attack is defined as that which occurs when the separated flow, which occurs at the sharp leading edge, mixes with the unseparated flow in a constant-area channel with no turning. This loss is, therefore, independent of solidity, camber, chord length, and blade thickness distribution downstream of the leading edge except insofar as these variables affect the flow direction just downstream of the blade leading edge. Stalling of the blades does not affect the validity of the equations derived herein within the limitations of the assumptions. The effect of stall is reflected in the magnitude of the flow deviation angle, which in this case would be the angle between the flow direction just downstream of the leading edge and the tangent to the blade camber line at that point. The numerical results

obtained assuming zero deviation angle represent the losses that would occur if the fluid were perfectly guided by the blades in the inlet region.

Thus the theoretical results indicate a maximum loss which would be decreased in an actual cascade because of the smaller amount of turning accomplished in the inlet section. Also, in an actual row of sharp-nosed blades, the blades will sustain some suction force before the flow separates. Therefore, the loss presented in this report represents a maximum pressure-loss limit, in two respects, toward which actual cascades of sharp-nosed blades tend.

If the flow direction is known by some means just downstream of the leading edge, then the deviation from the tangent to the camber line just downstream of the leading edge can be accounted for by substituting this known value of the deviation angle into the equations.

Equations are derived for the total- and static-pressure changes across the blade row as well as for the downstream velocity. These equations are derived for incompressible flow in the next section and for compressible flow in appendix B.

Incompressible Flow

In this section, the equations for the downstream velocity and the static- and total-pressure changes are derived for incompressible nonviscous flow. In the following analysis all variables are made dimensionless by expressing them as ratios of upstream-flow parameters. Thus, the velocity W with components U and V in the x- and y-directions (Cartesian coordinates), respectively; the static pressure p; the total pressure P; the blade force F_b, that is, the force exerted on the air by the blade; and the fluid weight density ρ are defined nondimensionally by the following equations (all symbols are defined in appendix A):

$$\left.\begin{aligned} W &= W'/W_1' \\ U &= U'/W_1' \\ V &= V'/W_1' \\ x &= x'/L \\ y &= y'/L \\ p &= p'/(P_1' - p_1') \\ P &= P'/(P_1' - p_1') \\ F_b &= F_b'/(P_1' - p_1')L \\ \rho &= \rho'/\rho_1' \end{aligned}\right\} \qquad (1)$$

The primed quantities refer to dimensional values, the subscript 1 refers to conditions far upstream of the cascade where flow conditions are uniform, and L is the distance normal to the x-axis between two adjacent stagnation streamlines far upstream of the cascade (fig. 2).

The quantities to be determined are the downstream velocity W_2, the static-pressure coefficient c_p, and the total-pressure loss coefficient $\bar{\omega}$. The superscript "bar" does not, of course, in this case indicate a vector quantity. The two coefficients c_p and $\bar{\omega}$ are defined as the dimensional static-pressure and total-pressure change, respectively, across the blade row divided by the difference between the upstream total and static pressure, or

$$c_p = \frac{p_2' - p_1'}{P_1' - p_1'} = p_2 - p_1 \tag{2a}$$

$$\bar{\omega} = \frac{P_1' - P_2'}{P_1' - p_1'} = P_1 - P_2 \tag{2b}$$

where the subscript 2 refers to conditions far downstream of the leading edge. Expressions for these quantities as functions of the geometry of the blade row are derived in the following analysis:

From the definition of nondimensional W and the fact that the flow is two dimensional, it follows that the equation of continuity is

$$\cos \beta_1 = W_2 \cos \beta_2 \tag{3}$$

where β is the angle between the x-direction and the flow direction (positive in the counterclockwise direction). The angle of attack α is defined as the difference between the upstream flow direction and the blade angle β_b, or

$$\alpha = \beta_1 - \beta_b \tag{4}$$

The deviation angle δ is the angle between the blade direction and the downstream flow direction, positive in the counterclockwise direction, or

$$\delta = \beta_2 - \beta_b \tag{5}$$

The subscript δ appended to $\bar{\omega}$ and c_p will indicate that the deviation angle is considered in the computation of that parameter. Thus, from equations (3), (4), and (5), it can be seen that $\cos \beta_1 / \cos(\beta_1 - \alpha + \delta)$

is greater than 1 for flow that is accelerated by the cascade and less than 1 for flow that is decelerated by the cascade.

In order to determine the change in static pressure from far upstream to far downstream, the momentum change across the blade row is considered. In figure 2 let DEFGHIJ be a control surface in the flow where DE and JI are adjacent stagnation streamlines, FG and HI are adjacent flat plates, F is the leading edge of the flat plate, E and I are stagnation points, and DJ and GH are normal to the x-direction far upstream and downstream, that is, at stations 1 and 2, respectively. Noting that for incompressible flow the difference between the upstream total and static pressures is equal to the upstream dynamic pressure, the momentum equation can be written nondimensionally in vector form as

$$\oint 2\rho \, d\bar{A} \cdot \bar{W} \, \bar{W} = - \oint p \, d\bar{A} \tag{6}$$

where $d\bar{A}$ is the nondimensional ratio of the differential area of the control surface to $L \times$unit span, and the superscript "bar" denotes a vector quantity. The surface integral on the left side of equation (6) is the flow of momentum across the control surface, and the line integral on the right is the resultant of the pressure forces acting on the fluid. The negative sign occurs because the pressure is inward, whereas the positive direction of the area vector is outward. There is, of course, no flow of momentum across the lines DEFG and HIJ since there is no velocity component normal to these lines. The sum of the integrals of the pressure forces along EFG and HI is equal to the blade force $\bar{F}_b$, whose scalar is a dimensionless quantity defined by equation (1). Thus,

$$\oint_{EFG} p \, d\bar{A} + \oint_{HI} p \, d\bar{A} = \bar{F}_b \tag{7}$$

The integral of the pressure forces from D to E is numerically equal but opposite in sign to the integral from I to J, or

$$\oint_{DE} p \, d\bar{A} = - \oint_{IJ} p \, d\bar{A} \tag{8}$$

Thus, these two parts of the complete line integral cancel each other.

Equation (5) can be split into components in the x- and y-directions. The equation for the momentum change in the x-direction is

$$\oint 2\rho WU \cos(\bar{n},\bar{W}) \, dA = - \oint p \cos(\bar{n},\bar{x}) \, dA \tag{9a}$$

and in the y-direction is

$$\oint 2\rho WV \cos(\bar{n},\bar{W})\, dA = -\oint p \cos(\bar{n},\bar{y})\, dA \tag{9b}$$

where $(\bar{n},\bar{W})$, $(\bar{n},\bar{x})$, and $(\bar{n},\bar{y})$ are the angles between the outer normal to the control-surface boundary and the flow direction, the x-axis, and the y-axis, respectively.

The density ρ is equal to 1 for incompressible flow, and the assumption has been made that the suction force on the blade nose is zero, that is, the blade force is normal to the blades. Therefore, by using the relations expressed in equations (7) and (8), equations (9a) and (9b) become, respectively,

$$F_b \sin(\beta_1 - \alpha) = p_2 - p_1 \tag{10a}$$

and

$$-F_b \cos(\beta_1 - \alpha) = 2 \cos \beta_1 \left[W_2 \sin(\beta_1 - \alpha + \delta) - \sin \beta_1\right] \tag{10b}$$

By combining equations (2a), (3), (4), (5), (10a), and (10b), the following equation for the dimensionless static-pressure change across the blade row, the static-pressure coefficient, is obtained:

$$c_{p,\delta} = \frac{2 \tan(\beta_1 - \alpha) \cos \beta_1 \sin(\alpha - \delta)}{\cos(\beta_1 - \alpha + \delta)} \tag{11}$$

Thus, the static-pressure coefficient is a function of the upstream flow angle, the angle of attack, and the deviation angle.

Bernoulli's equation for upstream and downstream conditions states that

$$P_1 = 1 + p_1 \tag{12a}$$

$$P_2 = W_2^2 + p_2 \tag{12b}$$

By means of equations (2b), (3), (4), (5), (11), (12a), and (12b), the total-pressure loss coefficient $\bar{\omega}_\delta$ is found to be given by

$$\bar{\omega}_\delta = 1 - \frac{2 \tan(\beta_1 - \alpha) \cos \beta_1 \sin(\alpha - \delta)}{\cos(\beta_1 - \alpha + \delta)} - \frac{\cos^2 \beta_1}{\cos^2(\beta_1 - \alpha + \delta)} \tag{13}$$

If δ is taken as zero, this expression for the total-pressure loss is equivalent to that obtained by Spannhake (ref. 3, pp. 129 and 150), which is

$$\bar{\omega} = \cos^2\beta_1\left[\tan\beta_1 - \tan(\beta_1 - \alpha)\right]^2$$

Spannhake's equation for the total-pressure loss coefficient was derived under the assumption that the total-pressure loss was equal to the kinetic energy associated with the velocity vector difference between the upstream and downstream velocities called the "shock" velocity in reference 3 and denoted by W_s in figure 3 of this report.

At the outset it was not apparent that the two approaches would lead to the same result. It appears that the approach used herein lends itself more readily to the development of the equations for compressible flow. The compressible case was not treated in reference 3.

Effect of δ. - The deviation angle δ cannot be predicted in general for flow of a real fluid. However, the deviation angle for incompressible potential flow can be obtained by means of the method described in reference 9. The results of the analysis presented in reference 9 indicate that

$$\delta = \tan^{-1}\left[\tan(\alpha + \beta_b) - \frac{2\varkappa \sin\alpha}{\cos(\alpha + \beta_b)\sqrt{\varkappa^4 + 2\varkappa^2\cos 2\beta_b + 1}}\right] - \beta_b \tag{14}$$

The parameter $\varkappa$ is related to the cascade solidity σ and the blade angle by the following equation:

$$\frac{\pi}{2}\sigma = \cos\beta_b \ln\frac{\sqrt{\varkappa^4 + 2\varkappa^2\cos 2\beta_b + 1} + 2\varkappa\cos\beta_b}{1 - \varkappa^2} + \sin\beta_b \tan^{-1}\frac{2\varkappa\sin\beta_b}{\sqrt{\varkappa^4 + 2\varkappa^2\cos 2\beta_b + 1}} \tag{15}$$

Thus, δ is a function of σ, β_1, and α, since β_b is related to β_1 and α by equation (4). The variation of δ with α for various values of β_1 and σ is shown in figure 4. The curve for β_1 equal to 80° extends only to α equals -5°, since the solution beyond this value is difficult to obtain and is of little interest.

The ratios $c_{p,\delta}/c_p$ and $\bar{\omega}_\delta/\bar{\omega}$ indicate the effects of δ in that these are the ratios of the pressure coefficients with δ taken into

account to the pressure coefficients with δ assumed zero. These ratios are given by the following equations for incompressible flow:

$$\frac{c_{p,\delta}}{c_p} = \frac{\sin(\alpha - \delta)\cos(\beta_1 - \alpha)}{\sin\alpha\cos(\beta_1 - \alpha + \delta)} \tag{16}$$

$$\frac{\varpi_\delta}{\varpi} = \frac{\cos^2(\beta_1-\alpha)\left[\cos^2(\beta_1-\alpha+\delta)-2\cos\beta_1\tan(\beta_1-\alpha)\sin(\alpha-\delta)\cos(\beta_1-\alpha+\delta)-\cos^2\beta_1\right]}{\cos^2(\beta_1-\alpha+\delta)\left[\cos^2(\beta_1-\alpha)-2\sin(\beta_1-\alpha)\cos\beta_1\sin\alpha-\cos^2\beta_1\right]} \tag{17}$$

As α approaches zero, δ also approaches zero and the right sides of equations (16) and (17) become indeterminate. These indeterminate forms were evaluated by L'Hospital's rule, and the following expressions were obtained for the limits approached by these functions as α approaches zero:

$$\lim_{\alpha\to 0} \frac{c_{p,\delta}}{c_p} = 1 - \frac{d\delta}{d\alpha} \tag{18}$$

$$\lim_{\alpha\to 0} \frac{\varpi_\delta}{\varpi} = 2\left(1 - \frac{d\delta}{d\alpha}\right) - \left(1 - \frac{d\delta}{d\alpha}\right)^2 \tag{19}$$

Equations (16), (17), (18), and (19) were solved with the use of the data shown in figure 4. The results of these calculations are shown in figures 5 and 6. These results are merely indications of the trends and the order of magnitude of the effects of δ, since the values of δ used were obtained assuming potential flow. Figures 5 and 6 indicate a marked increase in the effect of δ as the cascade solidity decreases below 1.0.

Compressible Flow

In appendix B an analysis is carried out for subsonic compressible flow similar to that for incompressible flow. The final equations are presented in the following section:

Equations. - The expression for the downstream Mach number M_2 is

$$M_2^2 = \frac{-B + \sqrt{B^2 + 4A}}{2A} \tag{20a}$$

in which

$$A = \frac{\frac{\gamma-1}{2}}{1 + \frac{\gamma-1}{2} M_1^2}\left[\frac{\cos(\beta_1 - \alpha + \delta)}{M_1 \cos \beta_1} + \frac{\gamma M_1 \cos(\beta_1 - \alpha + \delta) \cos \alpha}{\cos(\beta_1 - \alpha)}\right]^2 - \gamma^2 \frac{\cos^2 \delta \cos^2(\beta_1 - \alpha + \delta)}{\cos^2(\beta_1 - \alpha)}$$

$$B = \frac{1}{1 + \frac{\gamma-1}{2} M_1^2}\left[\frac{\cos(\beta_1 - \alpha + \delta)}{M_1 \cos \beta_1} + \frac{\gamma M_1 \cos(\beta_1 - \alpha + \delta) \cos \alpha}{\cos(\beta_1 - \alpha)}\right]^2 - 2\gamma \frac{\cos \delta \cos(\beta_1 - \alpha + \delta)}{\cos(\beta_1 - \alpha)} \qquad (20b)$$

Thus the downstream Mach number is seen to be a function of the upstream Mach number in addition to the upstream flow angle, angle of attack, and deviation angle.

When the downstream Mach number has been obtained from equations (20a) and (20b), the static-pressure coefficient can be found by means of the following equation:

$$c_{p,\delta} = \frac{\frac{M_1 \cos \beta_1}{M_2 \cos(\beta_1 - \alpha + \delta)}\left(\frac{1 + \frac{\gamma-1}{2} M_1^2}{1 + \frac{\gamma-1}{2} M_2^2}\right)^{1/2} - 1}{\left(1 + \frac{\gamma-1}{2} M_1^2\right)^{\frac{\gamma}{\gamma-1}} - 1} \qquad (21)$$

Because M_2 is a function of the upstream flow conditions and the deviation angle, it can be seen from equation (21) that the static-pressure coefficient also is a function of the upstream flow conditions and the deviation angle.

The quantity c_p is a ratio of the static-pressure change across the blade row to the difference between the upstream total and static pressures. For the incompressible case, this ratio is the same as the ratio of the static-pressure change to the upstream velocity head. However, for compressible flow, the upstream velocity head is a function

not only of the difference between the upstream total and static pressures but also the upstream Mach number. The static-pressure coefficient $c_{p,q}$ expressed as a ratio of the upstream velocity head is defined by

$$c_{p,q} = (p_2' - p_1') \Big/ \frac{\rho_1'(W_1')^2}{2g} \tag{22}$$

where g is the acceleration due to gravity. From this definition it can be seen that c_p is related to $c_{p,q}$ as follows:

$$\frac{c_{p,q}}{c_p} = (P_1' - p_1') \Big/ \frac{\rho_1'(W_1')^2}{2g} \tag{23}$$

The right side of equation (23) is a function of M_1 and is given by

$$(P_1' - p_1') \Big/ \frac{\rho_1'(W_1')^2}{2g} = \frac{\left(1 + \frac{\gamma-1}{2} M_1^2\right)^{\frac{\gamma}{\gamma-1}} - 1}{\frac{\gamma}{2} M_1^2} \tag{24}$$

The variation of this function with M_1 is shown in figure 7. This function $c_{p,q}/c_p$ is independent of any effects of δ as is obvious from its definition.

The total-pressure loss coefficient $\bar{\omega}$ can be found from the following equation, which is derived in appendix B:

$$\bar{\omega}_\delta = \frac{1 - \frac{M_1 \cos \beta_1}{M_2 \cos(\beta_1 - \alpha + \delta)} \left(\frac{1 + \frac{\gamma-1}{2} M_2^2}{1 + \frac{\gamma-1}{2} M_1^2} \right)^{\frac{\gamma+1}{2(\gamma-1)}}}{1 - \left(1 + \frac{\gamma-1}{2} M_1^2\right)^{\frac{\gamma}{1-\gamma}}} \tag{25}$$

Similar to the case for c_p, a total-pressure loss coefficient expressed as a ratio of the upstream velocity head can be defined as follows:

$$\bar{\omega}_q = (P_1' - P_2') \Big/ \frac{\rho_1'(W_1')^2}{2g} \tag{26}$$

The expression for the ratio $\bar{\omega}_q/\bar{\omega}$ is the same as that for $c_{p,q}/c_p$ given in equation (23). The variation of this function with M_1 is given by equation (24) and is shown in figure 7.

Effect of δ. - A considerably more elaborate computation is required to obtain the compressible potential-flow deviation angles than was required for the incompressible case. Consequently, it is not practical to compute even approximately the effect of δ as was done for incompressible flow. However, the effect of δ is probably of the same order of magnitude for compressible flow as for incompressible flow.

Limiting case. - The equations for compressible flow listed in the section Equations are limited to a certain range of upstream flow conditions, because the equation for M_2 yields imaginary values after a certain angle of attack is exceeded for a given M_1 and β_1. This angle of attack, called the critical angle of attack α_{cr}, is shown in appendix C to be that angle which results in a downstream Mach number equal to 1.0 (choking over the area ED, fig. 2) and is related to M_1 and β_1 by the following equation for the case where δ is equal to zero:

$$\sin^2\alpha_{cr}\left[(1+\gamma M_1^2)^2+\tan^2\beta_1\right]+\sin\alpha_{cr}\left[-2M_1\tan\beta_1\sqrt{2(\gamma+1)\left(1+\frac{\gamma-1}{2}M_1^2\right)}\right]+$$

$$\left[2M_1^2(\gamma+1)\left(1+\frac{\gamma-1}{2}M_1^2\right)-(1+\gamma M_1^2)^2\right]=0 \qquad (27)$$

Equation (27) can be solved by the quadratic formula for the critical angle of attack α_{cr} for a given M_1 and β_1. The variation of α_{cr} with M_1 and β_1 is shown in figure 8. It should be noted that, if choking occurs in the throat formed between the flat plates by the separated flow, the maximum (absolute) value of α for which the analysis is valid may be less than that indicated by equation (27).

RESULTS AND DISCUSSIONS

The equations derived in the preceding analysis for $\bar{\omega}$ and c_p are solved for a range of upstream flow angle β_1 and angle of attack α for incompressible flow and for a range of β_1, α, and upstream Mach number M_1 for compressible flow. The deviation angle δ is assumed to be zero in all these calculations. These results are presented in a series of figures showing the variation of total-pressure loss and static-pressure coefficients with β_1 and α for the incompressible

case and with β_1, α, and M_1 for the compressible case. As previously indicated in the section Preliminary Considerations, the total-pressure losses obtained by this method represent an upper limit toward which the losses in an actual cascade of sharp-nosed blades tend.

Incompressible Flow

In figure 9 the variation of total-pressure loss coefficient with angle of attack is presented for various values of upstream flow angle and for zero deviation angle. Except for the case of β_1 equal to zero, which is symmetrical, the total-pressure loss is always greater for negative α than for numerically equal positive α. This condition is accentuated as β_1 increases. The range of operation at negative α for a given permissible loss in total pressure is greatly reduced as β_1 is increased. For positive α, there is little variation in total-pressure loss with upstream flow angle as β_1 varies from zero to 60°.

The variation of the static-pressure coefficient with angle of attack for various values of upstream flow angle is presented in figure 10. Again the curve for β_1 equal to zero is symmetrical, and c_p is always zero or negative. This results from the fact that, for β_1 equal to zero, the fluid is accelerated in passing through the blade row for any nonzero angle of attack.

Two factors affect the static-pressure coefficient. Any loss in total pressure tends to lower the static pressure if the velocity head remains the same. Also, for a given total pressure, the static pressure decreases as the velocity head increases and conversely (see eq. (12b)). Thus, when the fluid is accelerated, that is, W_2 is greater than 1, the static pressure decreases; and when the fluid is decelerated, that is, W_2 is less than 1, the static pressure increases except in cases where this is offset by a loss in total pressure. Consider, for example, the curve for β_1 equal to 20°. It indicates a zero static-pressure coefficient when α is equal to 20°. Equation (3) indicates that the flow is decelerated for such an upstream flow angle and angle of attack. This would tend to cause a static-pressure rise, but this is offset by the total-pressure loss indicated in figure 9. For β_1 of 20° and α of 30°, the total-pressure loss is so great that the static-pressure coefficient becomes negative even though the flow is decelerated.

For all values of β_1 the curves reach a maximum, beyond which further increases in α cause decreases in c_p. The curve for β_1 equal to 80° reaches a maximum at a comparatively small positive angle of attack; and at an angle of attack of 30°, c_p is less than the

corresponding value for β_1 equal to 60°. These phenomena occur for the same reason as discussed in the preceding paragraph.

Compressible Flow

The variation of the total-pressure loss coefficient $\bar{\omega}$ for compressible flow with upstream flow angle, upstream Mach number, and angle of attack is shown in figure 11. On each plot β_1 is constant, and the variation of $\bar{\omega}$ with α for various values of M_1 is shown. The curve for M_1 equal to zero is that for incompressible flow. It will be noted that not all the curves extend over the entire range of angle of attack shown on the abscissa. The end points of these curves occur at the critical angles of attack, the angles of attack which result in sonic downstream velocity. The variation of this critical angle of attack with β_1 and M_1 is shown in figure 8.

For all values of β_1, the values of $\bar{\omega}$ become greater as M_1 increases. The effect of M_1 in increasing $\bar{\omega}$ becomes more pronounced as β_1 increases and is greater for negative angles of attack than for positive. In general, the effect of M_1 in increasing $\bar{\omega}$ for positive α is negligible. However, it should be noted that $\bar{\omega}$ is a dimensionless ratio of $(P_1' - p_1')$. If $\bar{\omega}$ were expressed as a dimensionless ratio of $\rho_1'(W_1')^2/2g$, on the other hand, figure 7 indicates that $\bar{\omega}$ would increase appreciably with M_1. As β_1 increases, the range of operation at negative α decreases in such manner that for β_1 of 80°, a negative α of less than 1° causes the system to choke when M_1 is 0.8.

The variation of the static-pressure coefficient c_p with β_1, M_1, and α is presented in figure 12. In general, the effect of M_1 on c_p is greater than its effect on $\bar{\omega}$.

For β_1 equal to 20°, the total-pressure losses are sufficiently large that, although the geometry of the cascade indicates a decelerating flow for incompressible flow, M_2 increases and eventually the flow chokes downstream at α of about 26° for M_1 equal to 0.8. Consequently, for β_1 equal to 20° and α greater than 15°, c_p decreases as M_1 increases. The decrease in c_p with increasing M_1 also occurs at α greater than 8° for β_1 equal to 80°. This same trend, that is, decreasing c_p as M_1 increases, is approached by the curves for β_1 equal to 40° and 60° at large α. This trend causes the maximum value of c_p to occur for smaller α as M_1 increases.

SUMMARY OF RESULTS AND CONCLUSIONS

A method of computing the losses in total pressure caused by a nonzero angle of attack at the inlet to a row of sharp-nosed blades is developed for both incompressible and subsonic compressible flow. The method is based on momentum considerations across a row of zero-thickness flat plates. The results of the analysis are presented in a series of figures showing the variation of the total-pressure loss coefficient $\bar{\omega}$ and the static-pressure coefficient c_p with upstream flow angle β_1 and angle of attack α for incompressible flow and with β_1, α, and upstream Mach number M_1 for compressible flow. The downstream flow deviation angle was assumed to be zero in all cases for the computations. These figures and the equations from which they were obtained indicate for the range of variables and conditions considered that:

1. Increases in β_1 cause sharp rises in $\bar{\omega}$ and corresponding drops in c_p for negative α, but for positive α and β_1 less than 60° there is little variation in $\bar{\omega}$ with β_1.

2. Increases in M_1 cause only slightly higher values of $\bar{\omega}$ for positive α.

3. A maximum value of c_p occurs for a given value of β_1 at a certain positive value of α, beyond which further increases in α result in decreases in c_p due to total-pressure losses. The value of α at which this maximum c_p occurs decreases as M_1 increases.

Lewis Flight Propulsion Laboratory
National Advisory Committee for Aeronautics
Cleveland, Ohio, July 20, 1954

APPENDIX A

SYMBOLS

The following symbols are used in this report:

A,B	functions of M_1, β_1, α, and δ (eq. (20b))
a	local speed of sound
C	function of M_1, β_1, α, and δ (eq. (C1))
c_p	static-pressure coefficient, nondimensional (eq. (2a))
$c_{p,q}$	static-pressure coefficient expressed as nondimensional ratio of upstream dynamic pressure (eq. (22))
DEFGHIJ	points around control surface, fig. 2
dA	differential element of control-surface area, nondimensional
F_b	blade force, nondimensional (eq. (1))
g	acceleration due to gravity
L	distance normal to x-axis between adjacent stagnation streamlines, dimensional
M	Mach number, nondimensional
n	unit normal to control surface, positive direction is outward
P	total pressure, nondimensional (eq. (1))
p	static pressure, nondimensional (eq. (1))
R	gas constant
T	total temperature
t	static temperature
U	velocity component in x-direction, nondimensional (eq. (1))
V	velocity component in y-direction, nondimensional (eq. (1))

W	resultant velocity, nondimensional (eq. (1))
x,y	Cartesian coordinates, nondimensional (eq. (1))
α	angle of attack (eq. (4))
β	flow direction, positive in counterclockwise direction from positive x-axis
β_b	blade direction, positive in counterclockwise direction from positive x-axis
γ	ratio of specific heats
δ	flow deviation angle, angle between blade direction and downstream flow direction, positive in counterclockwise direction from blade direction (eq. (5))
ρ	fluid weight density, nondimensional (eq. (1))
$\bar{\omega}$	total-pressure loss, expressed as nondimensional ratio of $P_1' - p_1'$ (eq. (2b))
$\bar{\omega}_q$	total-pressure loss, expressed as nondimensional ratio of upstream dynamic pressure (eq. (26))

Subscripts:

1	conditions infinite distance upstream of cascade
2	conditions downstream of leading edge
cr	conditions when M_2 is equal to 1.0
s	shock component of velocity as in ref. 3 (see fig. 3 of this report)
δ	flow deviation angle taken into account

Superscripts:

'	dimensional value of quantity
$-$	vector quantity

CT-3

APPENDIX B

DEVELOPMENT OF EQUATIONS FOR COMPRESSIBLE FLOW

For compressible flow, the equations for the momentum change in the x- and y-directions become, respectively,

$$F_b' \sin(\beta_1-\alpha)-(p_2'-p_1')L = \frac{\rho_1'M_1a_1 \cos \beta_1 L}{g}\left[M_2a_2 \cos(\beta_1-\alpha+\delta) - M_1a_1 \cos \beta_1\right] \tag{B1}$$

and

$$-F_b' \cos(\beta_1 - \alpha) = \frac{\rho_1'M_1a_1 \cos \beta_1 L}{g}\left[M_2a_2 \sin(\beta_1 - \alpha + \delta) - M_1a_1 \sin \beta_1\right] \tag{B2}$$

where a is the local speed of sound. These two equations are solved simultaneously to yield

$$p_1' - p_2' = \frac{\rho_1'M_1a_1 \cos \beta_1}{g \cos(\beta_1 - \alpha)} (M_2a_2 \cos \delta - M_1a_1 \cos \alpha) \tag{B3}$$

In addition to the momentum equation, equation (B3), the following four equations, which are the equation of state, equation of continuity, energy equation, and speed-of-sound equation, respectively, are known:

$$p' = \rho' Rt \tag{B4}$$

$$\rho_1'M_1a_1 \cos \beta_1 = \rho_2'M_2a_2 \cos(\beta_1 - \alpha + \delta) \tag{B5}$$

$$\frac{T}{t} = 1 + \frac{\gamma-1}{2} M^2 \tag{B6}$$

$$a^2 = \gamma g R t \tag{B7}$$

In these equations t is the static temperature; T, the total temperature; R, the gas constant; and γ, the ratio of specific heats. Thus, equations (B3), (B4), (B5), (B6), and (B7) form a system of five equations in the five unknowns p_2, ρ_2, t_2, M_2, and a_2. The total temperature T is constant since no work is done on the fluid. Combining equations (B4), (B5), and (B7) results in

$$\frac{p_2'}{p_1'} = \frac{M_1 \cos \beta_1}{M_2 \cos(\beta_1 - \alpha + \delta)} \left(\frac{1 + \frac{\gamma-1}{2} M_1^2}{1 + \frac{\gamma-1}{2} M_2^2} \right)^{1/2} \tag{B8}$$

Combining equations (B3), (B4), and (B7) results in

$$1 - \frac{p_2'}{p_1'} = \frac{\gamma M_1 \cos \beta_1}{\cos(\beta_1 - \alpha)} \left[M_2 \left(\frac{1 + \frac{\gamma-1}{2} M_1^2}{1 + \frac{\gamma-1}{2} M_2^2} \right)^{1/2} \cos \delta - M_1 \cos \alpha \right] \tag{B9}$$

Combining equations (B8) and (B9) results in

$$\left[1 + \frac{\gamma M_1^2 \cos \beta_1 \cos \alpha}{\cos(\beta_1 - \alpha)} \right] M_2 \left(\frac{1 + \frac{\gamma-1}{2} M_2^2}{1 + \frac{\gamma-1}{2} M_1^2} \right)^{1/2}$$

$$= \frac{M_1 \cos \beta_1}{\cos(\beta_1 - \alpha + \delta)} + \gamma \frac{\cos \beta_1 M_1 M_2^2 \cos \delta}{\cos(\beta_1 - \alpha)} \tag{B10}$$

Squaring both sides of equation (B10) and combining like terms result in

$$M_2^4 \left\{ \frac{\frac{\gamma-1}{2}}{1 + \frac{\gamma-1}{2} M_1^2} \left[\frac{\cos(\beta_1 - \alpha + \delta)}{M_1 \cos \beta_1} + \frac{\gamma M_1 \cos(\beta_1 - \alpha + \delta) \cos \alpha}{\cos(\beta_1 - \alpha)} \right]^2 - \gamma^2 \frac{\cos^2 \delta \cos^2(\beta_1 - \alpha + \delta)}{\cos^2(\beta_1 - \alpha)} \right\} +$$

$$M_2^2 \left\{ \frac{1}{1 + \frac{\gamma-1}{2} M_1^2} \left[\frac{\cos(\beta_1 - \alpha + \delta)}{M_1 \cos \beta_1} + \frac{\gamma M_1 \cos(\beta_1 - \alpha + \delta) \cos \alpha}{\cos(\beta_1 - \alpha)} \right]^2 - 2\gamma \frac{\cos \delta \cos(\beta_1 - \alpha + \delta)}{\cos(\beta_1 - \alpha)} \right\} - 1$$

$$= 0 \tag{B11}$$

This equation can be solved by the quadratic formula as follows:

$$M_2^2 = \frac{-B + \sqrt{B^2 + 4A}}{2A} \tag{20a}$$

where

$$\left.\begin{aligned} A = \frac{\frac{\gamma-1}{2}}{1+\frac{\gamma-1}{2}M_1^2}\left[\frac{\cos(\beta_1-\alpha+\delta)}{M_1\cos\beta_1}+\frac{\gamma M_1\cos(\beta_1-\alpha+\delta)\cos\alpha}{\cos(\beta_1-\alpha)}\right]^2 - \\ \gamma^2\frac{\cos^2\delta\cos^2(\beta_1-\alpha+\delta)}{\cos^2(\beta_1-\alpha)} \end{aligned}\right\} \quad (20b)$$

$$\left.\begin{aligned} B = \frac{1}{1+\frac{\gamma-1}{2}M_1^2}\left[\frac{\cos(\beta_1-\alpha+\delta)}{M_1\cos\beta_1}+\frac{\gamma M_1\cos(\beta_1-\alpha+\delta)\cos\alpha}{\cos(\beta_1-\alpha)}\right]^2 - \\ 2\gamma\frac{\cos\delta\cos(\beta_1-\alpha+\delta)}{\cos(\beta_1-\alpha)} \end{aligned}\right\}$$

Only the positive sign is shown before the radical in equation (20a) because the negative sign results either in imaginary values of M_2 or in real values of M_2 that indicate a decrease in the entropy of the fluid in passing through the blade row. Neither of these is admissible.

Equations (20a) and (20b) determine the downstream Mach number M_2 as a function of the upstream Mach number, the flow direction, the angle of attack, and the downstream flow deviation angle. When M_2 is obtained, the static-pressure coefficient, which is defined as

$$c_{p,\delta} = \frac{p_2' - p_1'}{P_1' - p_1'} = \frac{(p_2'/p_1') - 1}{(P_1'/p_1') - 1}$$

can be obtained. The ratio p_2'/p_1' can be expressed as a function of the assumed known quantities by means of equation (B8). The total pressure at a point is the pressure that the fluid would assume if it were decelerated isentropically to a stagnation condition. Therefore,

$$\frac{P_1'}{p_1'} = \left(1+\frac{\gamma-1}{2}M_1^2\right)^{\frac{\gamma}{\gamma-1}} \quad (B12)$$

The static-pressure coefficient thus becomes

$$c_{p,\delta} = \frac{\dfrac{M_1 \cos \beta_1}{M_2 \cos(\beta_1 - \alpha + \delta)} \left(\dfrac{1 + \frac{\gamma-1}{2} M_1^2}{1 + \frac{\gamma-1}{2} M_2^2} \right)^{1/2} - 1}{\left(1 + \frac{\gamma-1}{2} M_1^2 \right)^{\frac{\gamma}{\gamma-1}} - 1} \tag{21}$$

In order to obtain $c_{p,q}$ (see eq. (22)) from c_p, it is necessary to know the ratio of the difference between the dimensional upstream total and static pressures to the dimensional upstream velocity head (see eq. (23)). This ratio can be expressed as

$$\frac{P_1' - p_1'}{\rho_1'(W_1')^2/2g} = \frac{(P_1'/p_1') - 1}{\rho_1'(W_1')^2/2p_1'g} \tag{B13}$$

Equation (B13) can be simplified to obtain

$$\frac{P_1' - p_1'}{\rho_1'(W_1')^2/2g} = \frac{\left(1 + \frac{\gamma-1}{2} M_1^2 \right)^{\frac{\gamma}{\gamma-1}} - 1}{\frac{\gamma}{2} M_1^2} \tag{24}$$

Equation (24) can be used to relate $c_{p,q}$ to c_p.

The total-pressure loss coefficient is defined as

$$\bar{\omega}_\delta = \frac{P_1' - P_2'}{P_1' - p_1'} = \frac{(P_1'/p_1') - (P_2'/p_1')}{(P_1'/p_1') - 1}$$

In order to express $\bar{\omega}_\delta$ as a function of the assumed known variables, it is necessary to find an expression for P_2'/p_1' only, since P_1'/p_1' is given by equation (B12).

Noting the identity

$$\frac{P_2'}{p_1'} = \frac{P_2'}{p_2'} \frac{p_2'}{p_1'}$$

and using equations (B8), (B10), and the equation corresponding to equation (B12) at station 2 result in

$$\frac{P_2'}{P_1'} = \frac{M_1 \cos \beta_1}{M_2 \cos(\beta_1 - \alpha + \delta)} \left(\frac{1 + \frac{\gamma-1}{2} M_1^2}{1 + \frac{\gamma-1}{2} M_2^2} \right)^{1/2} \left(1 + \frac{\gamma-1}{2} M_2^2 \right)^{\frac{\gamma}{\gamma-1}} \quad \text{(B14)}$$

Thus, the equation for $\bar{\omega}_\delta$ is

$$\bar{\omega}_\delta = \frac{1 - \frac{M_1 \cos \beta_1}{M_2 \cos(\beta_1 - \alpha + \delta)} \left(\frac{1 + \frac{\gamma-1}{2} M_2^2}{1 + \frac{\gamma-1}{2} M_1^2} \right)^{\frac{\gamma+1}{2(\gamma-1)}}}{1 - \left(1 + \frac{\gamma-1}{2} M_1^2 \right)^{\frac{\gamma}{1-\gamma}}} \quad (25)$$

APPENDIX C

DERIVATION OF EQUATION FOR CRITICAL ANGLE OF ATTACK

Equations (20a) and (20b) yield real values for the downstream Mach number M_2 for all values of α, β_1, δ, and M_1 such that

$$B^2 + 4A > 0$$

Let

$$C = \frac{1}{\left(1 + \frac{\gamma-1}{2} M_1^2\right)} \left[\frac{\cos(\beta_1 - \alpha + \delta)}{M_1 \cos \beta_1} + \frac{\gamma M_1 \cos(\beta_1 - \alpha + \delta) \cos \alpha}{\cos(\beta_1 - \alpha)} \right]^2 \tag{C1}$$

In order to solve for α_{cr}, that is, the angle of attack which if exceeded results in equation (20a) yielding imaginary roots for a given M_1 and β_1, $B^2 + 4A$ is set equal to zero and the resulting equation solved for α. The value of α obtained from this equation is α_{cr}. Thus

$$B^2 + 4A = 0 = (C - 2\gamma)^2 + 4\left(\frac{\gamma-1}{2} C - \gamma^2\right)$$

This equation simplifies to

$$C^2 - 2(\gamma+1) C = 0$$

which has the roots

$$C = 0$$

$$C = 2(\gamma+1)$$

If C is equal to zero, equation (20a) indicates that M_2^2 is negative. Zero, therefore, is an extraneous root. If C is equal to $2(\gamma+1)$, equation (20a) indicates that M_2 is equal to 1. The limiting condition, therefore, is reached when the downstream flow is choked. In order to find the relation among α_{cr}, M_1, and β_1, C is set equal to $2(\gamma+1)$ and the resulting equation solved for α. For a given β_1, δ is a function of α for a given cascade and is, therefore, not an independent variable. Thus,

$$\frac{1}{\left(1+\frac{\gamma-1}{2}M_1^2\right)}\left[\frac{\cos(\beta_1-\alpha_{cr}+\delta)}{M_1\cos\beta_1}+\frac{\gamma M_1\cos(\beta_1-\alpha_{cr}+\delta)\cos\alpha_{cr}}{\cos(\beta_1-\alpha_{cr})}\right]^2=2(\gamma+1)$$

If δ is assumed equal to zero, this equation yields the following quadratic equation for $\sin\alpha_{cr}$ which can be solved by the quadratic formula:

$$\sin^2\alpha_{cr}\left[(1+\gamma M_1^2)^2+\tan^2\beta_1\right]+\sin\alpha_{cr}\left[-2M_1\tan\beta_1\sqrt{2(\gamma+1)\left(1+\frac{\gamma-1}{2}M_1^2\right)}\right]+$$

$$\left[2M_1^2(\gamma+1)\left(1+\frac{\gamma-1}{2}M_1^2\right)-(1+\gamma M_1^2)^2\right]=0 \qquad (27)$$

REFERENCES

1. Milne-Thomson, L. M.: Theoretical Aerodynamics. D. Van Nostrand Co., Inc., 1947.

2. Hamrick, Joseph T., Mizisin, John, and Michel, Donald J.: Study of Three-Dimensional Internal Flow Distribution Based on Measurements in a 48-Inch Radial-Inlet Centrifugal Impeller. NACA TN 3101, 1954.

3. Spannhake, Wilhelm: Centrifugal Pumps, Turbines, and Propellers. The Technology Press, M.I.T. (Cambridge), 1934.

4. Stodola, A.: Steam and Gas Turbines. McGraw-Hill Book Co., Inc., 1927. (Reprinted, Peter Smith (New York), 1945.)

5. Kochendorfer, Fred D., and Nettles, J. Cary: An Analytical Method of Estimating Turbine Performance. NACA Rep. 930, 1949. (Supersedes NACA RM E8I16.)

6. Birkhoff, Garrett: Hydrodynamics. Princeton Univ. Press, 1950.

7. Greenhill, G.: Report on the Theory of a Stream Line Past a Plane Barrier, and of the Discontinuity Arising at the Edge, with an Application of the Theory to an Airplane. R. & M. No. 19, British A.R.C., 1910.

8. Michell, J. H.: On The theory of Free Stream Lines. Phil. Trans. Roy. Soc., ser. A, vol. 181, 1890, pp. 389-431.

9. Durand, William Frederick: Aerodynamic Theory. Vol. II. Durand Reprinting Comm. (C.I.T.), 1943, pp. 91-96.

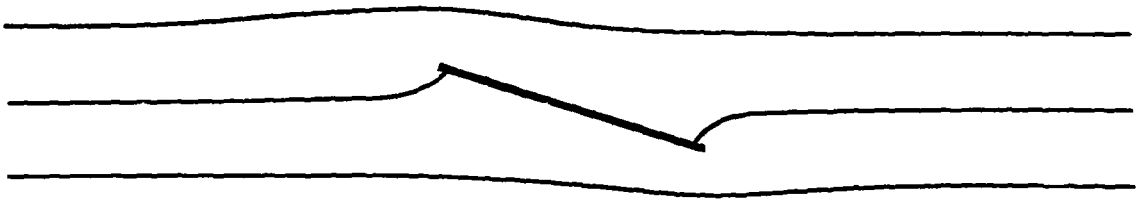

(a) Dirichlet flow.

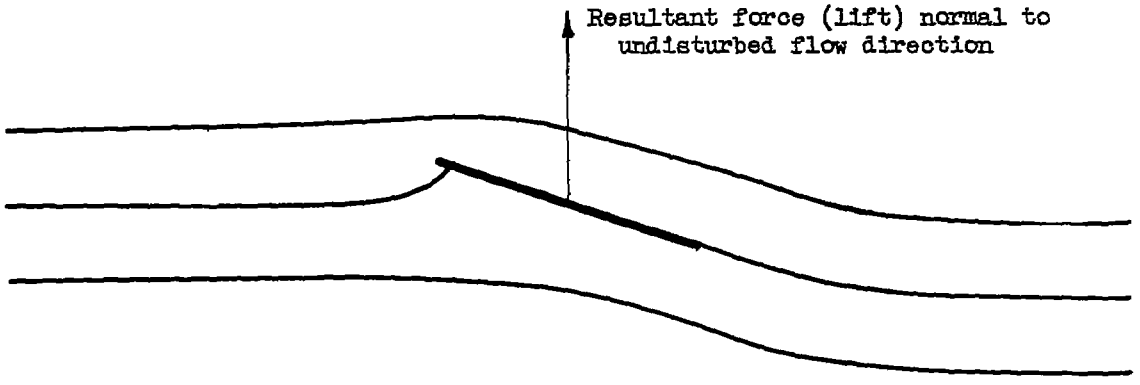

(b) Joukowski flow.

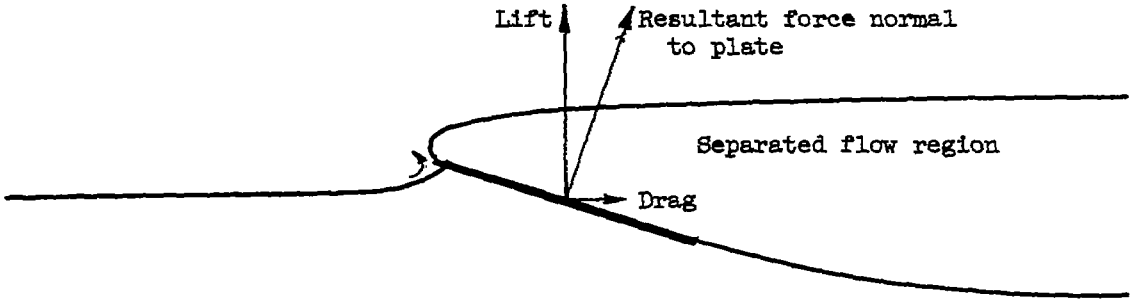

(c) Free-streamline flow.

Figure 1. - Three ideal flows past an inclined flat plate.

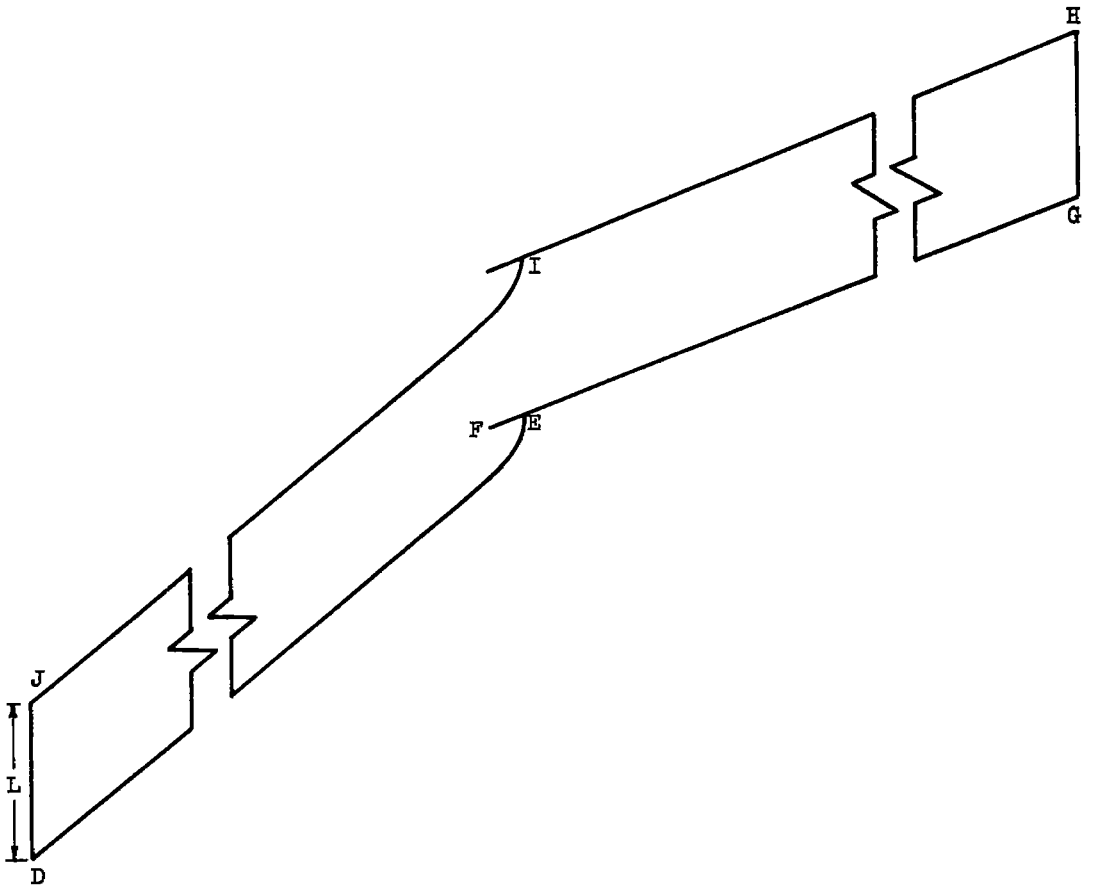

Figure 2. - Control surface in flow field.

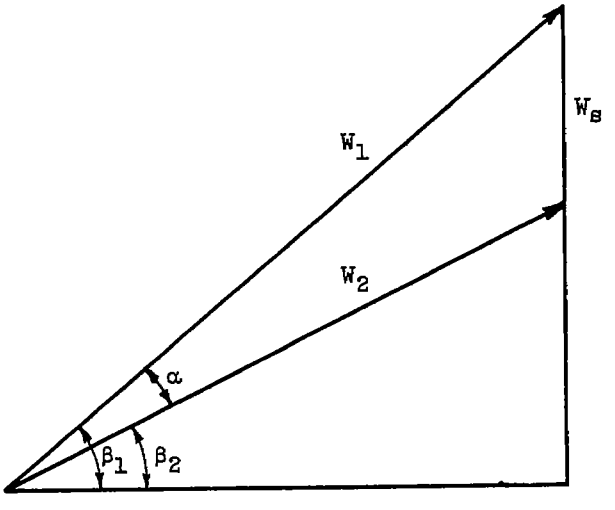

Figure 3. - Velocity vector diagram showing "shock" velocity component W_s of reference 3.

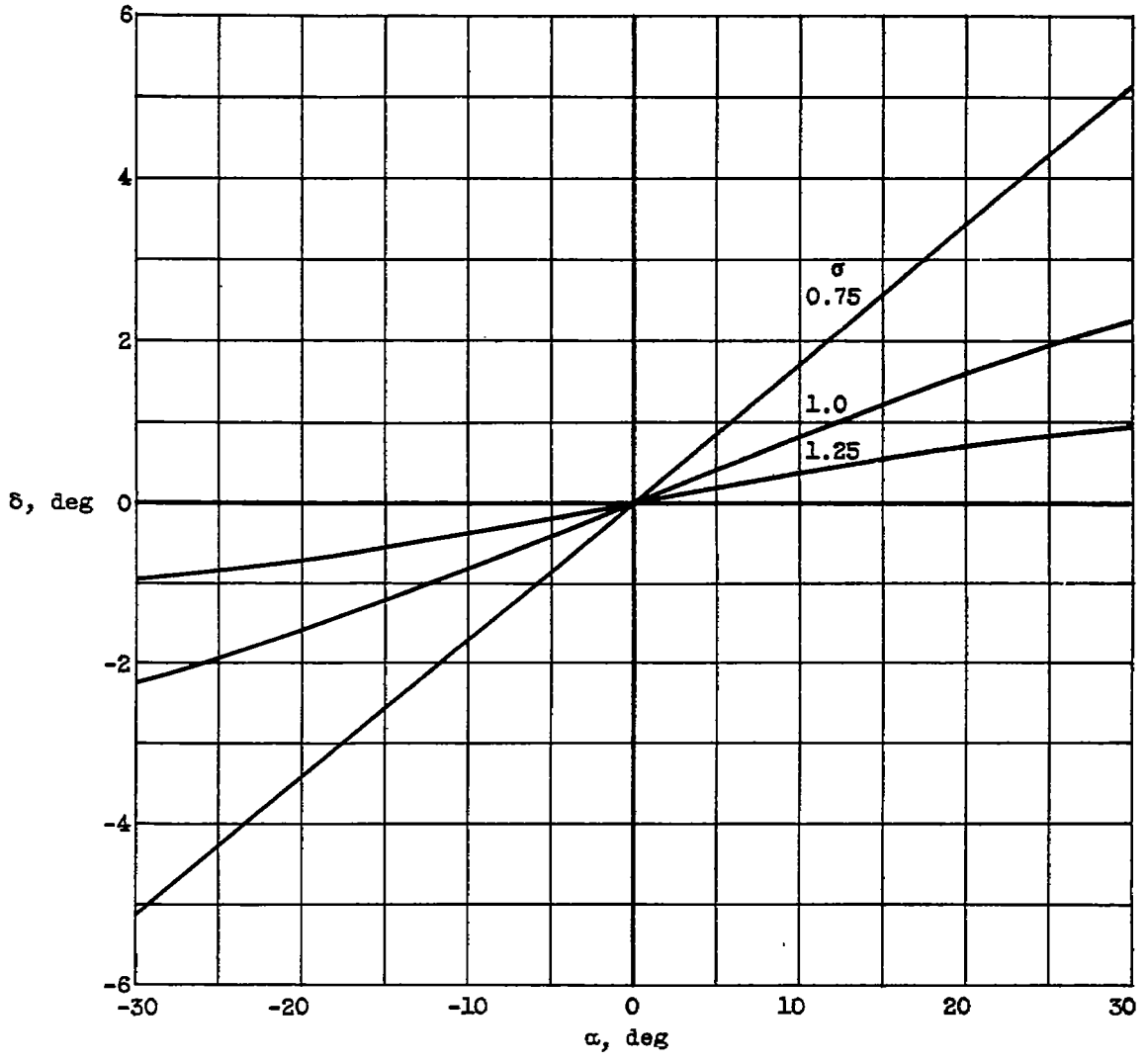

(a) β_1, 0.

Figure 4. - Variation of deviation angle δ with angle of attack α for various solidities σ and upstream flow angles β_1.

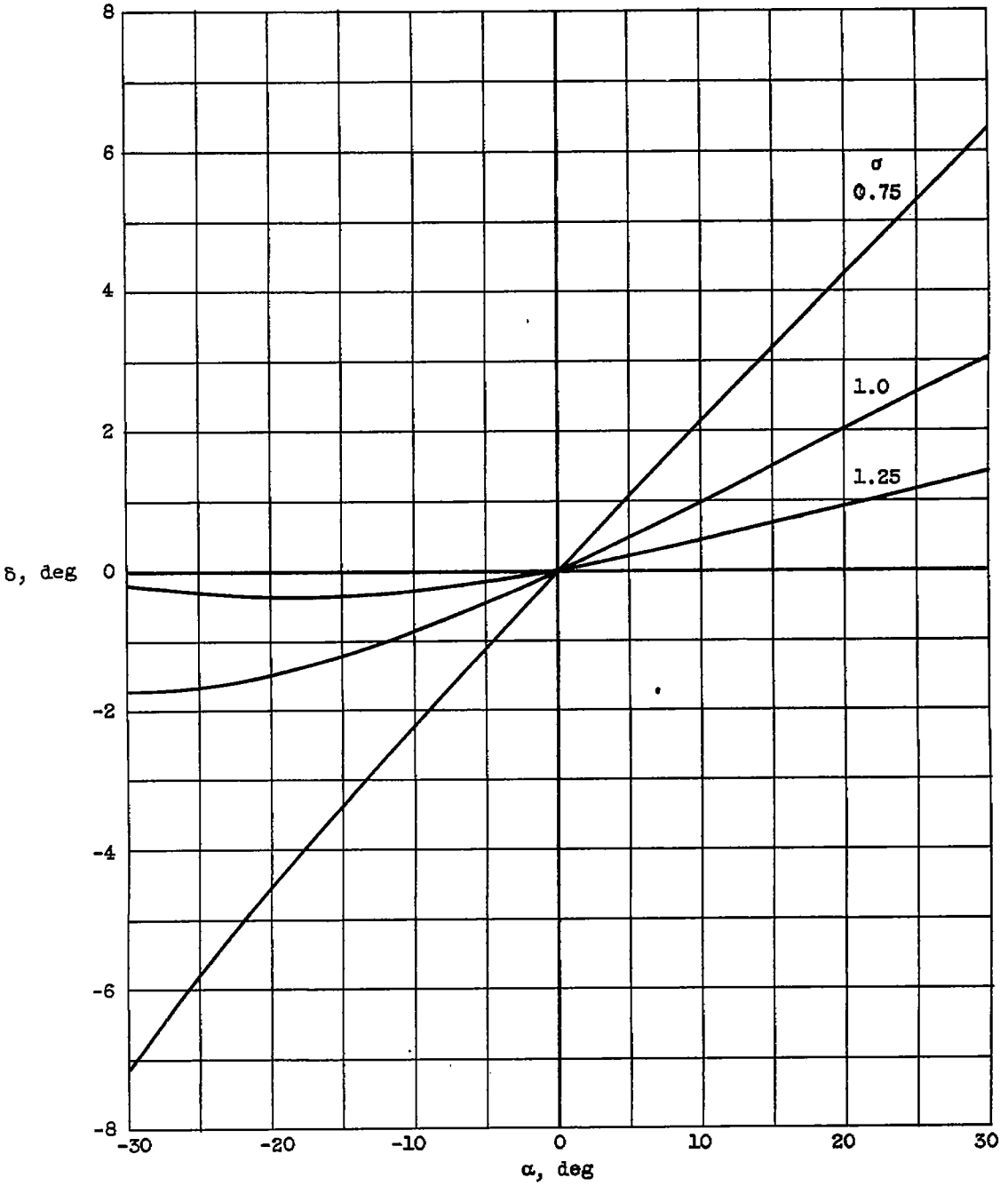

(b) β_1, 40°.

Figure 4. - Continued. Variation of deviation angle δ with angle of attack α for various solidities σ and upstream flow angles β_1.

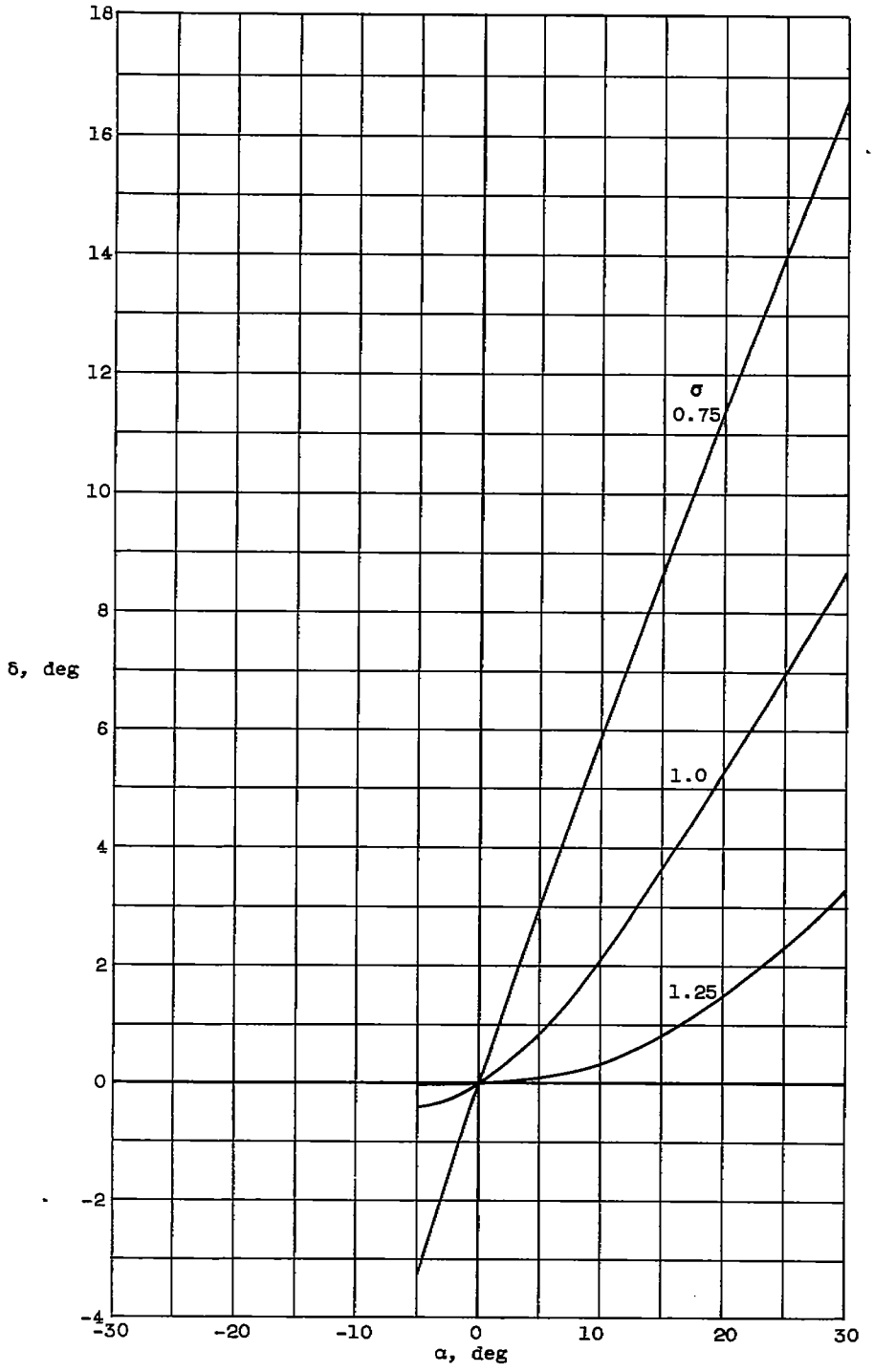

(c) β_1, 80°.

Figure 4. - Concluded. Variation of deviation angle δ with angle of attack α for various solidities σ and upstream flow angles β_1.

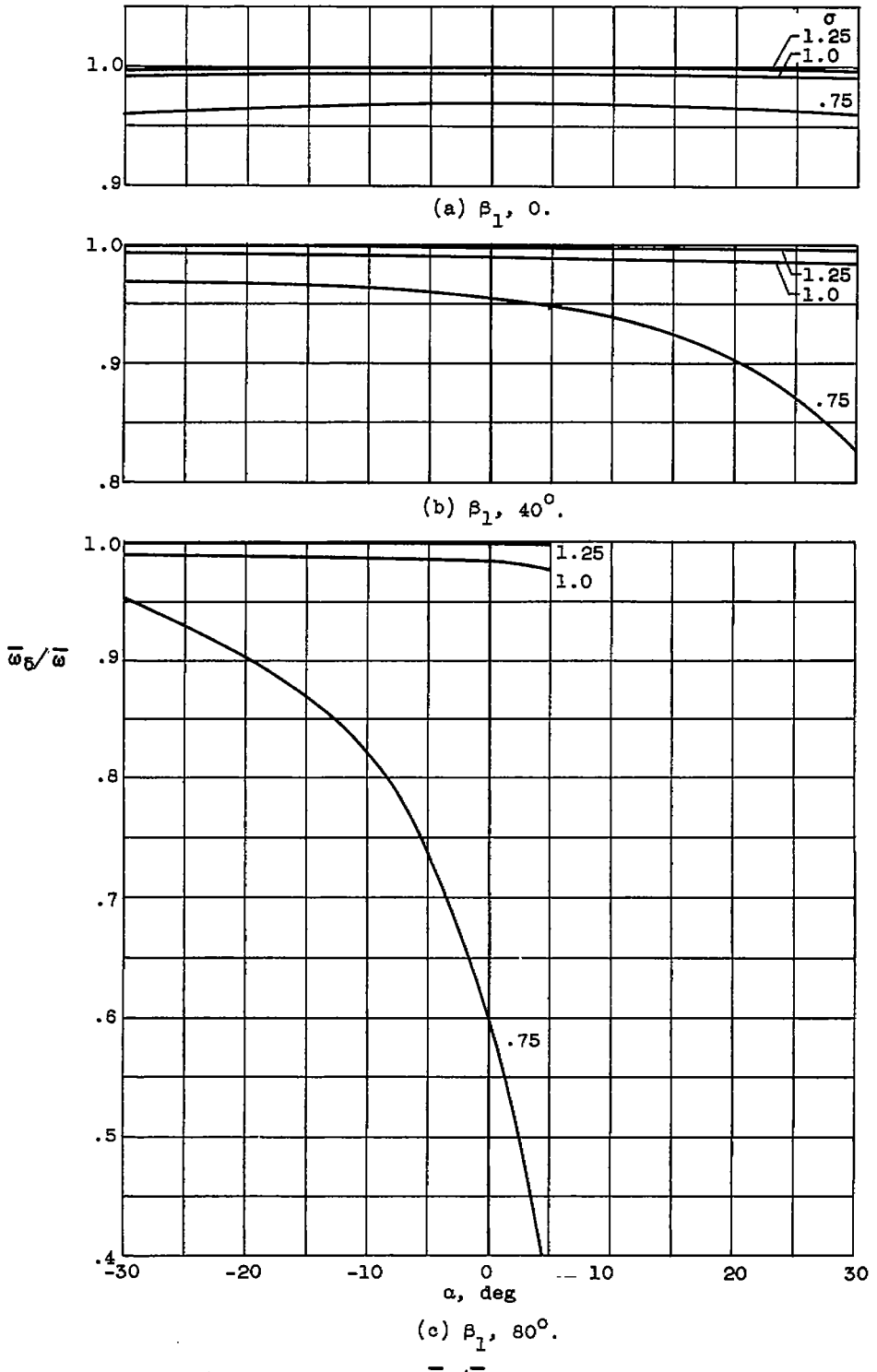

Figure 5. - Variation of $\overline{\omega}_\delta/\overline{\omega}$ with angle of attack α for various values of solidity σ and upstream flow angle β_1.

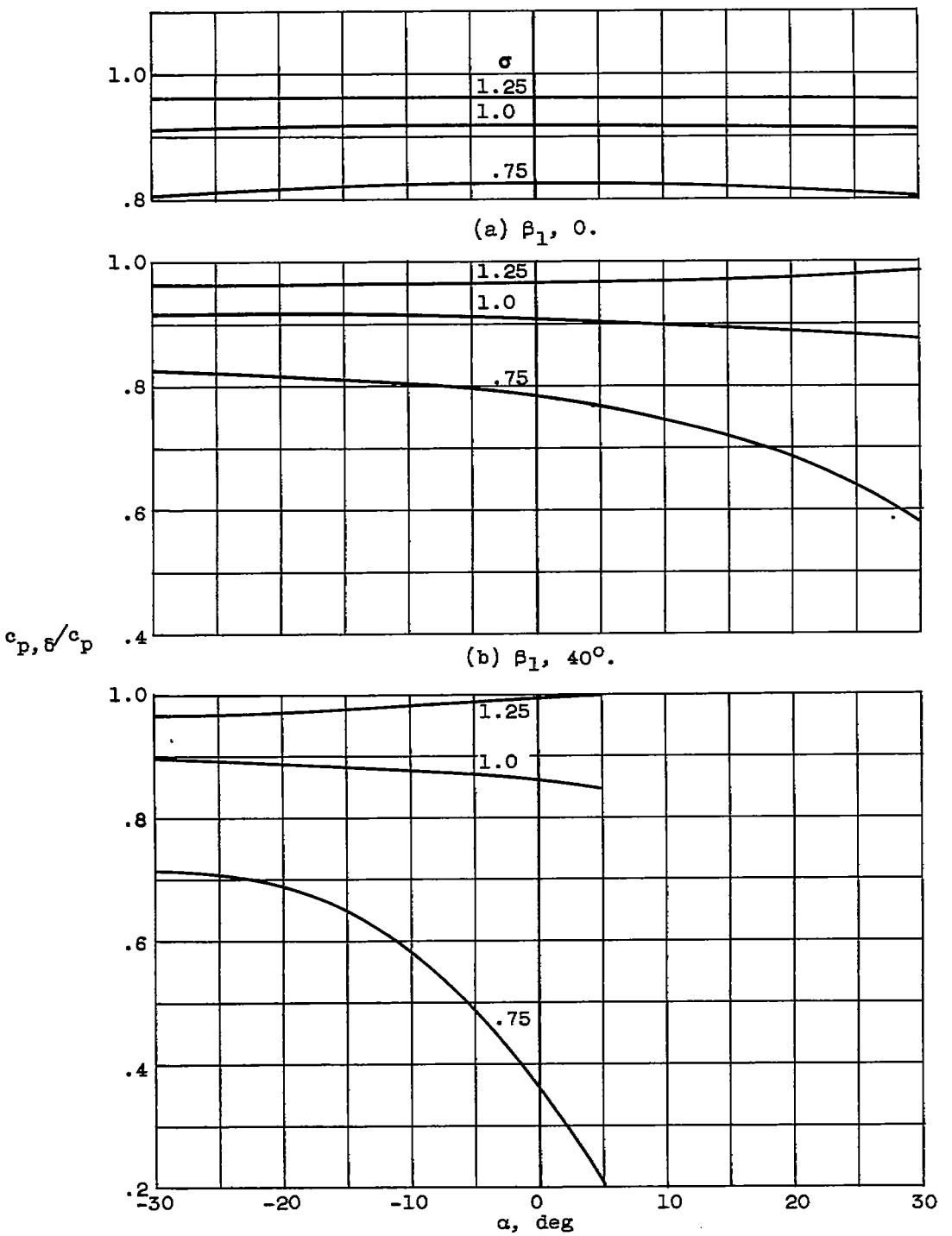

Figure 6. - Variation of $c_{p,\delta}/c_p$ with angle of attack α for various values of solidity σ and upstream flow angle β_1.

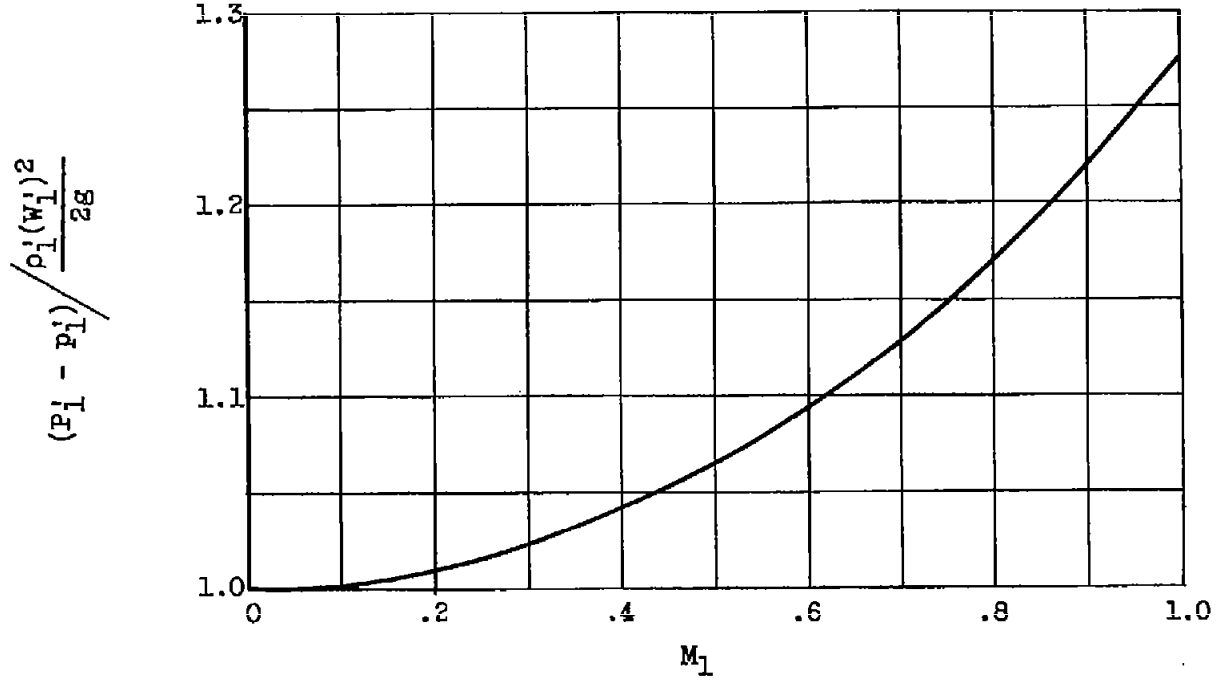

Figure 7. - Variation of ratio of upstream total and static pressure difference to upstream dynamic pressure $(P_1' - p_1')\Big/\frac{\rho_1'(W_1')^2}{2g}$ with upstream Mach number M_1.

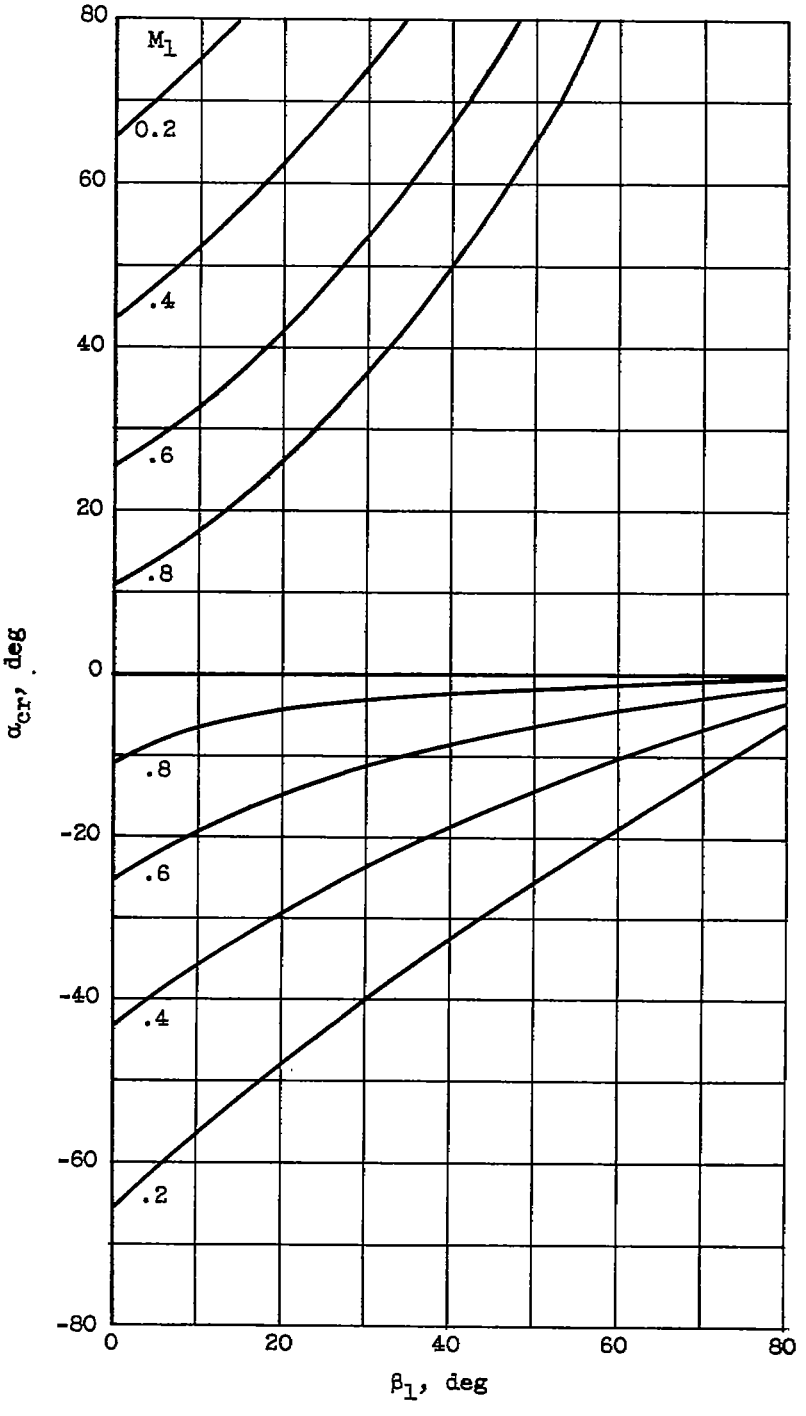

Figure 8. - Variation of critical angle of attack α_{cr} with upstream flow angle β_1 for various values of upstream Mach number M_1. Downstream flow deviation angle δ assumed equal to zero.

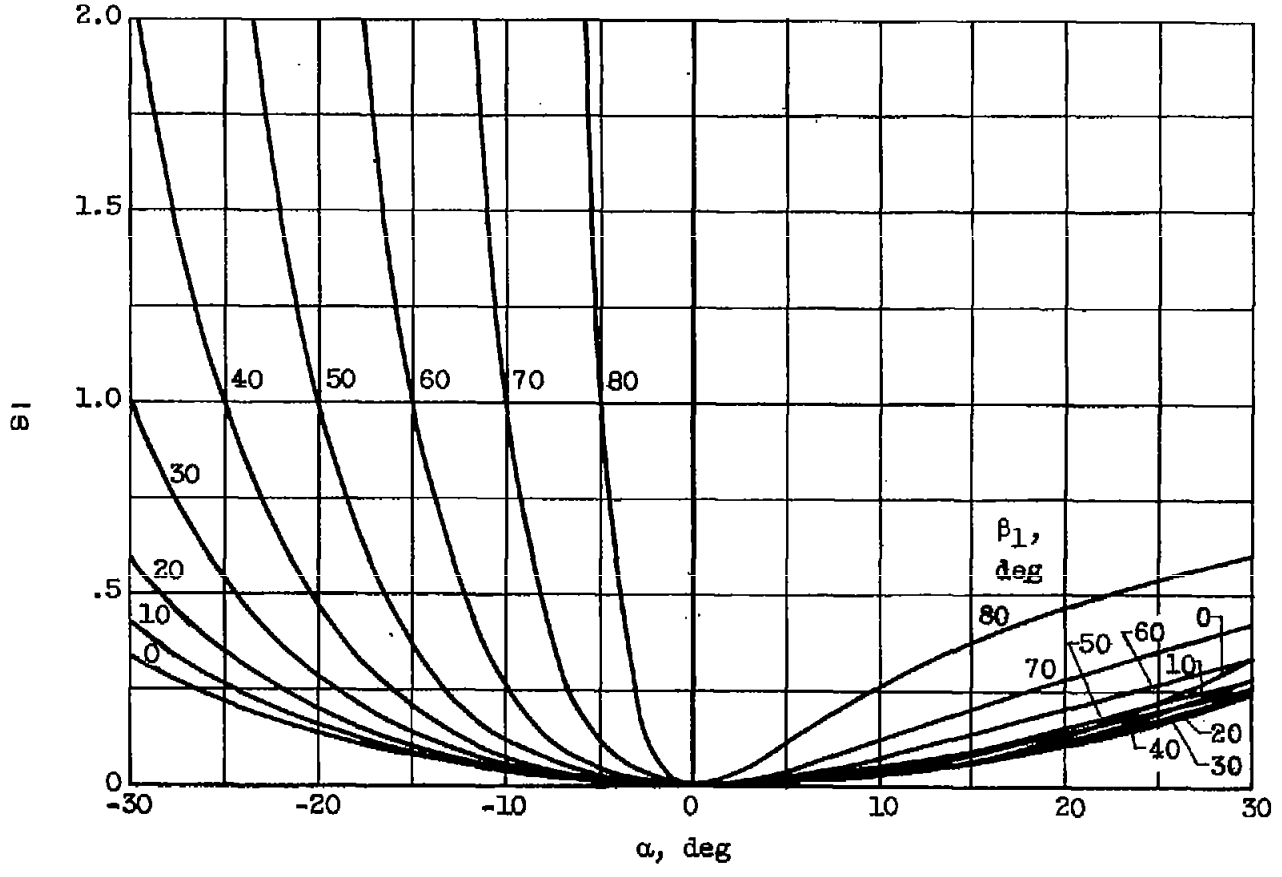

Figure 9. - Variation of total-pressure loss coefficient $\bar{\omega}$ with angle of attack α for various values of upstream flow angle β_1 for incompressible flow. Downstream flow deviation angle δ assumed equal to zero.

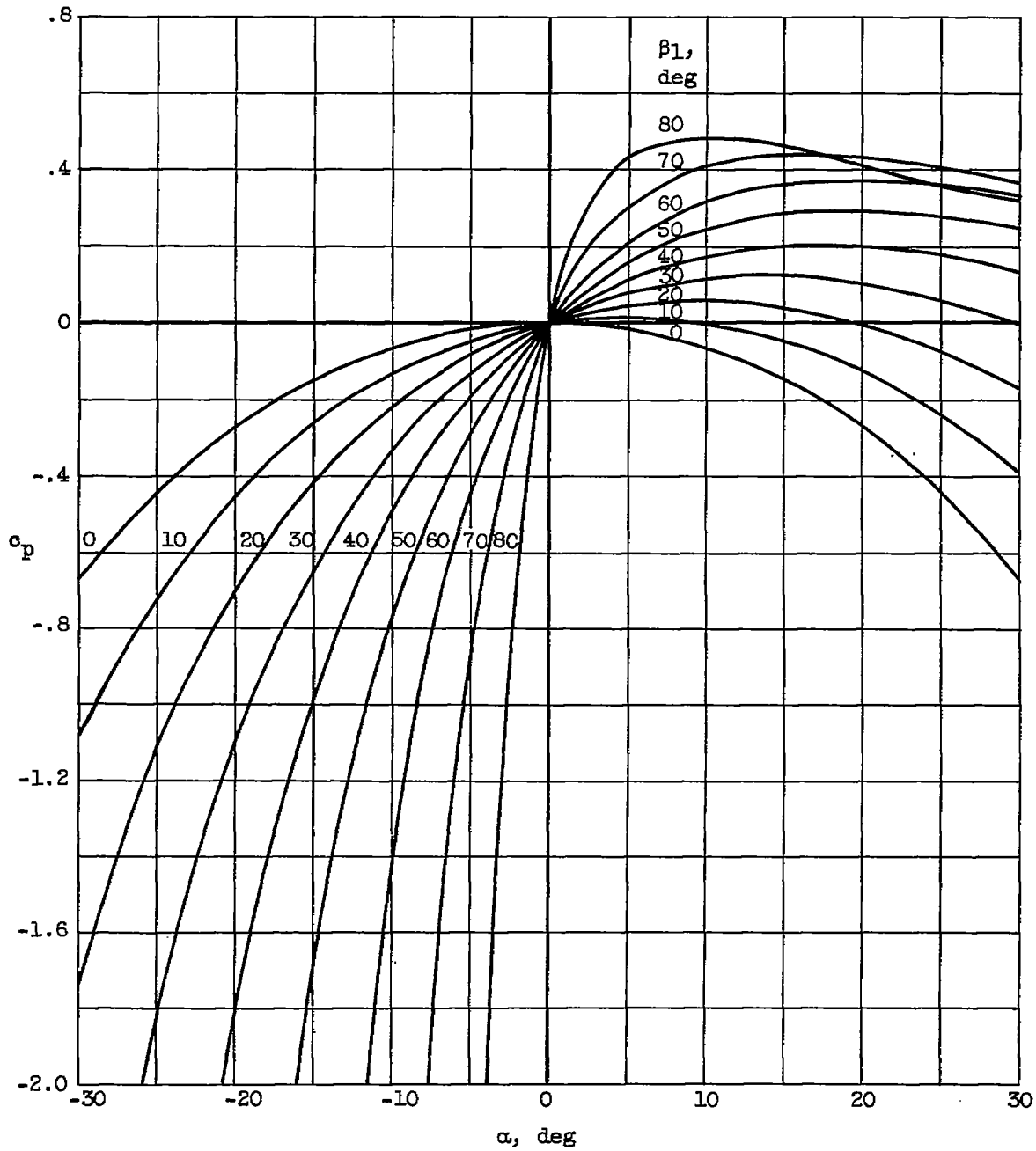

Figure 10. - Variation of static-pressure coefficient c_p with angle of attack α for various values of upstream flow angle β_1 for incompressible flow. Downstream flow deviation angle δ assumed equal to zero.

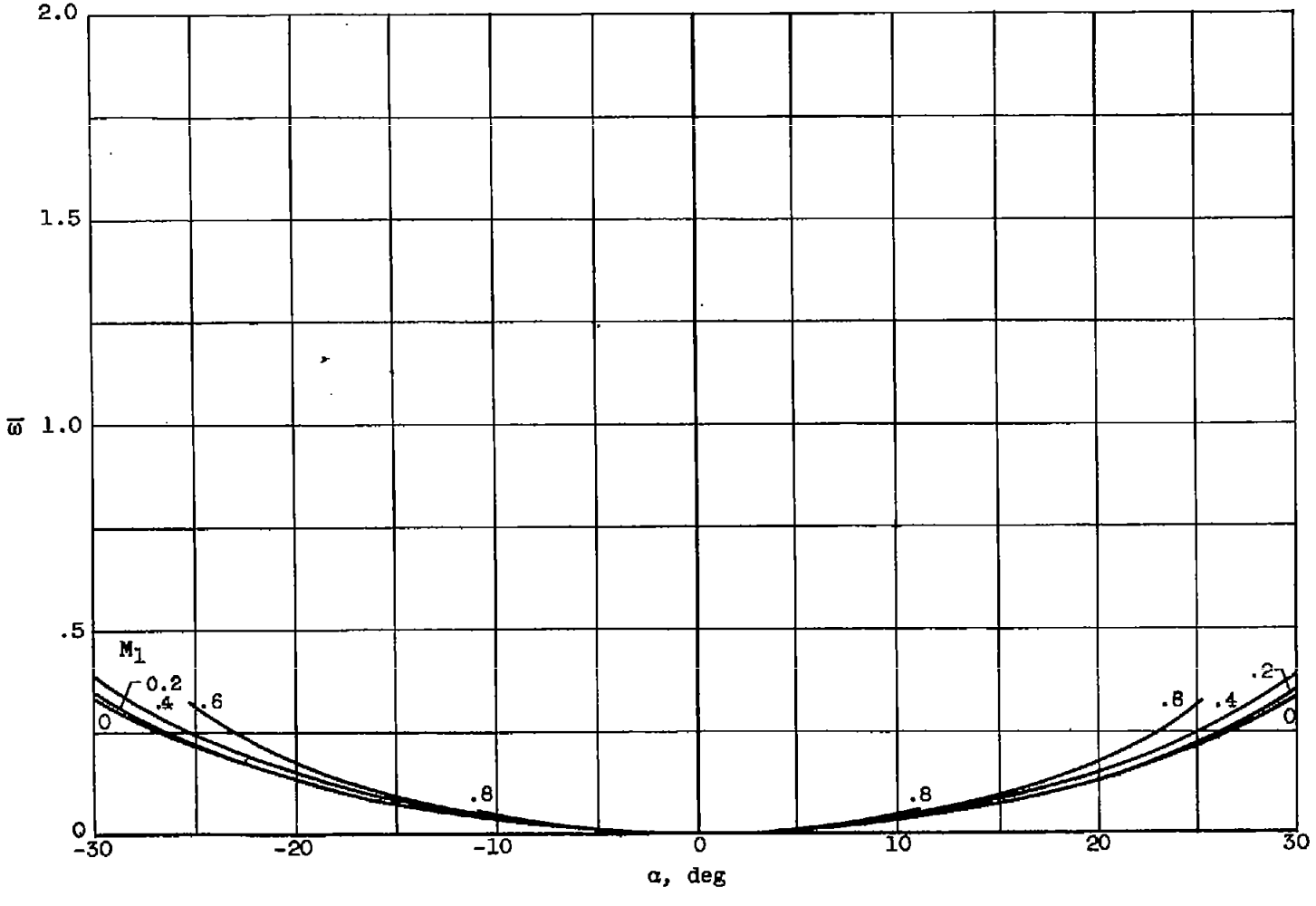

(a) β_1, 0.

Figure 11. - Variation of total-pressure loss coefficient $\bar{\omega}$ with angle of attack α for various values of upstream flow angle β_1 and upstream Mach number M_1. Downstream flow deviation angle δ assumed equal to zero.

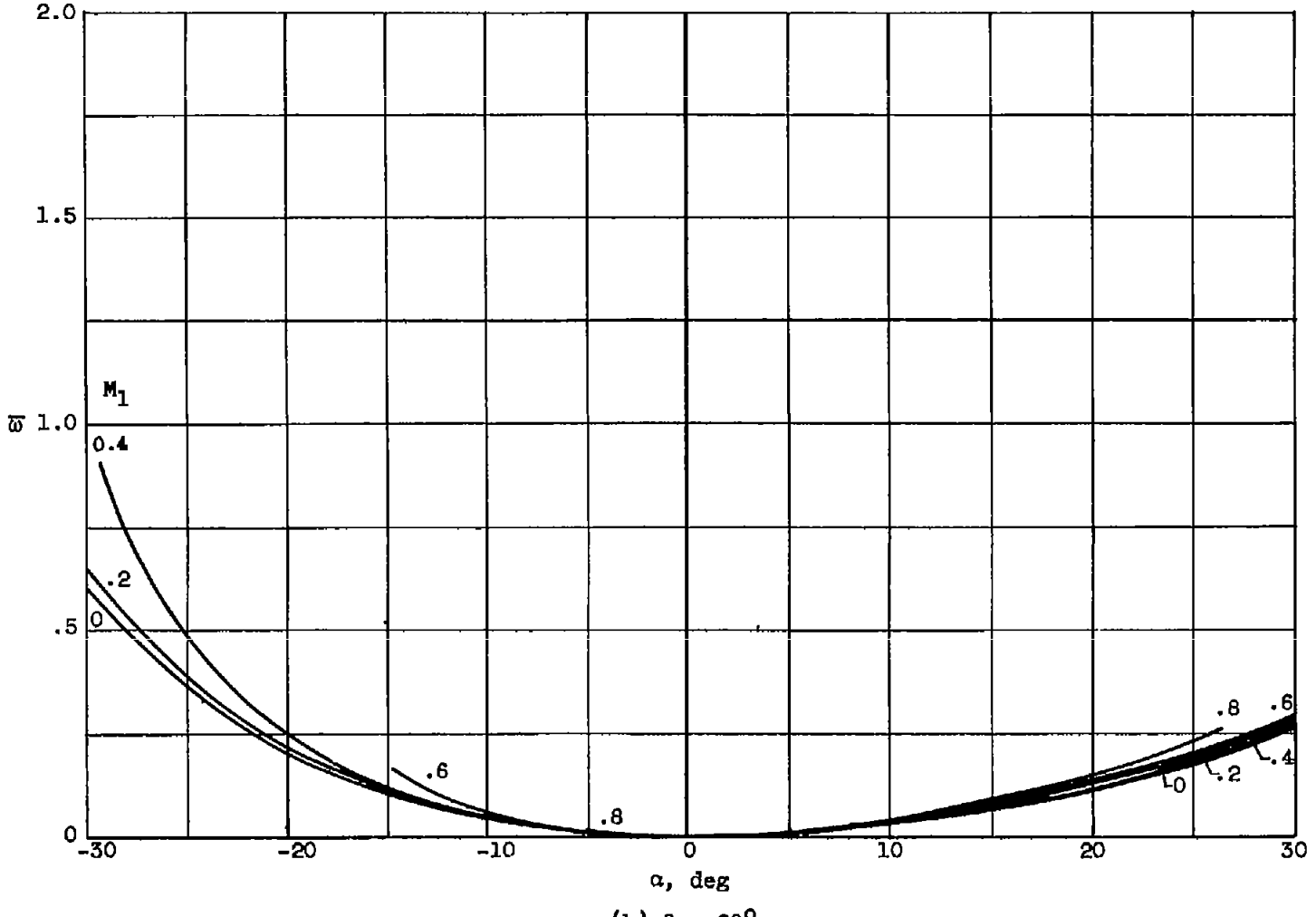

(b) β_1, 20°.

Figure 11. - Continued. Variation of total-pressure loss coefficient $\bar{\omega}$ with angle of attack α for various values of upstream flow angle β_1 and upstream Mach number M_1. Downstream flow deviation angle δ assumed equal to zero.

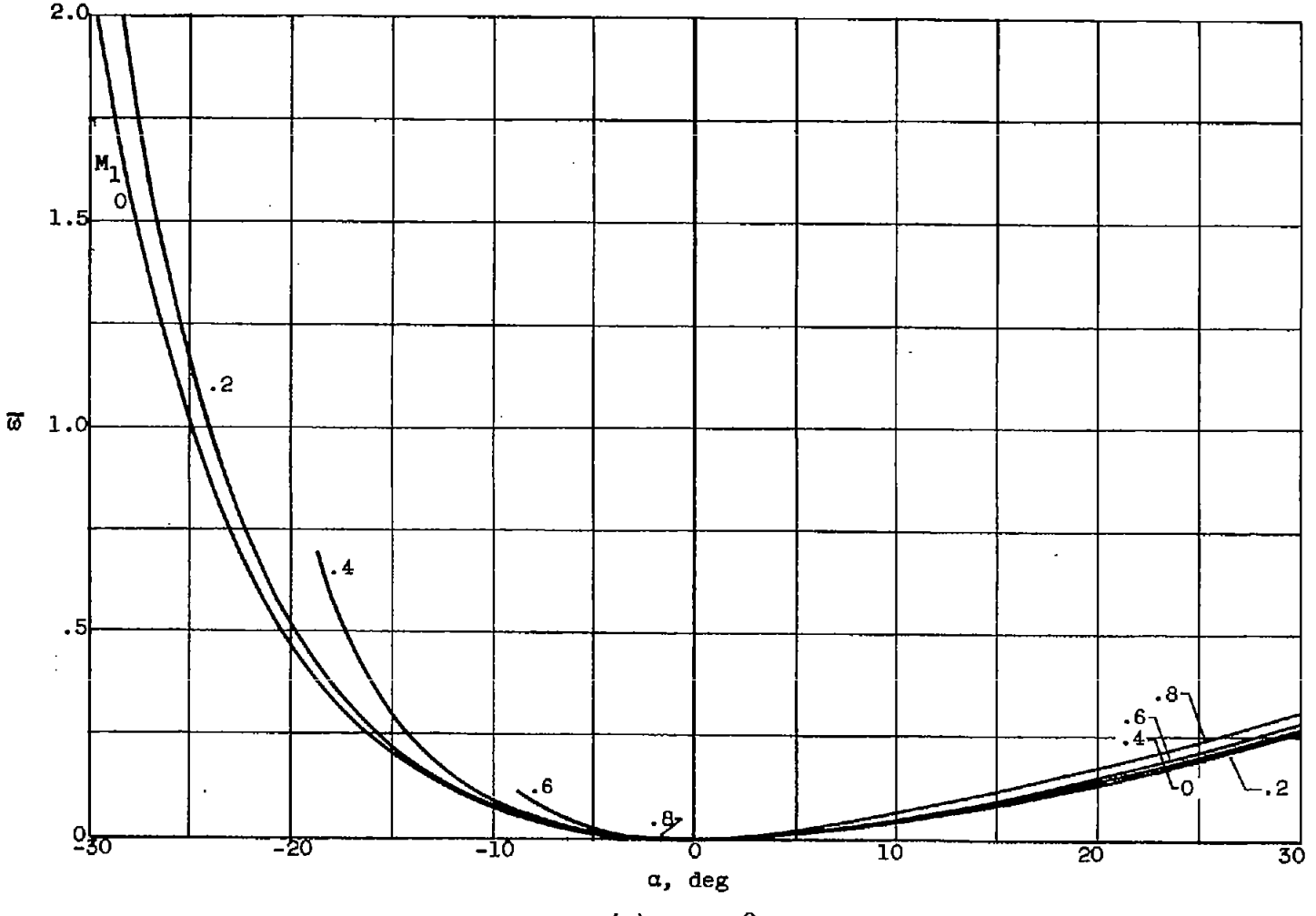

(c) β_1, 40°.

Figure 11. - Continued. Variation of total-pressure loss coefficient $\bar{\omega}$ with angle of attack α for various values of upstream flow angle β_1 and upstream Mach number M_1. Downstream flow deviation angle δ assumed equal to zero.

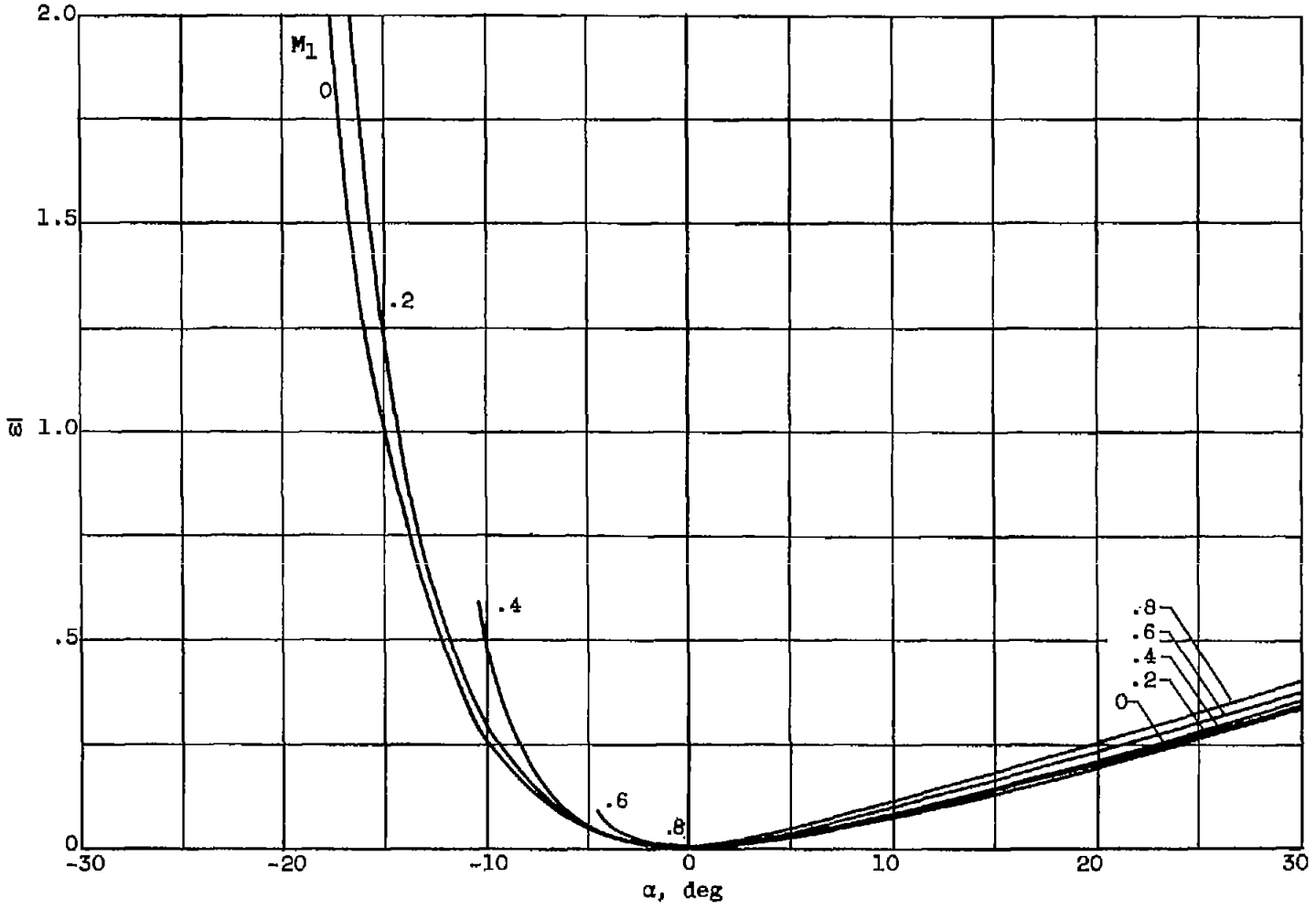

(d) β_1, 60°.

Figure 11. - Continued. Variation of total-pressure loss coefficient $\bar{\omega}$ with angle of attack α for various values of upstream flow angle β_1 and upstream Mach number M_1. Downstream flow deviation angle δ assumed equal to zero.

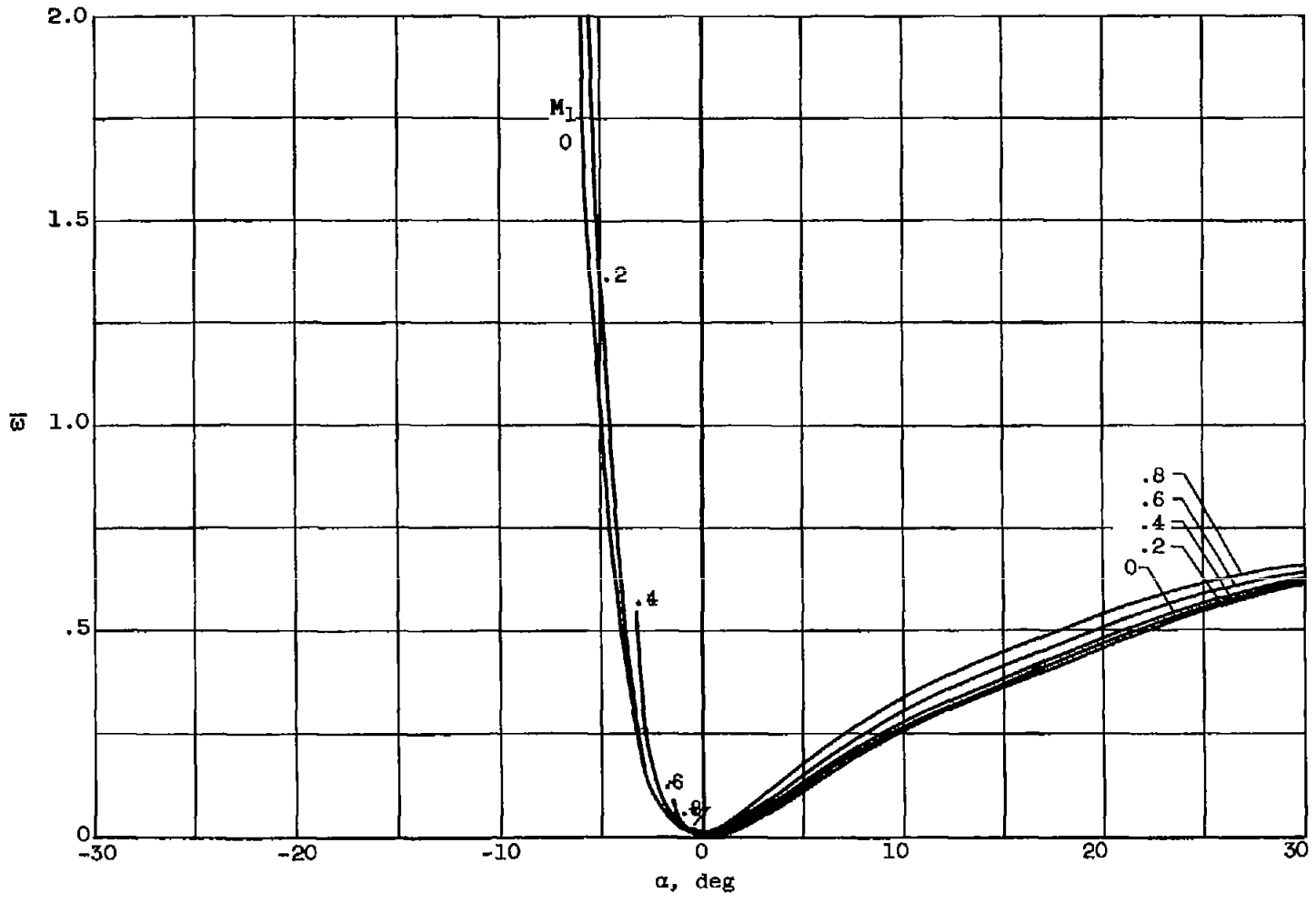

(e) β_1, 80°.

Figure 11. - Concluded. Variation of total-pressure loss coefficient $\bar{\omega}$ with angle of attack α for various values of upstream flow angle β_1 and upstream Mach number M_1. Downstream flow deviation angle δ assumed equal to zero.

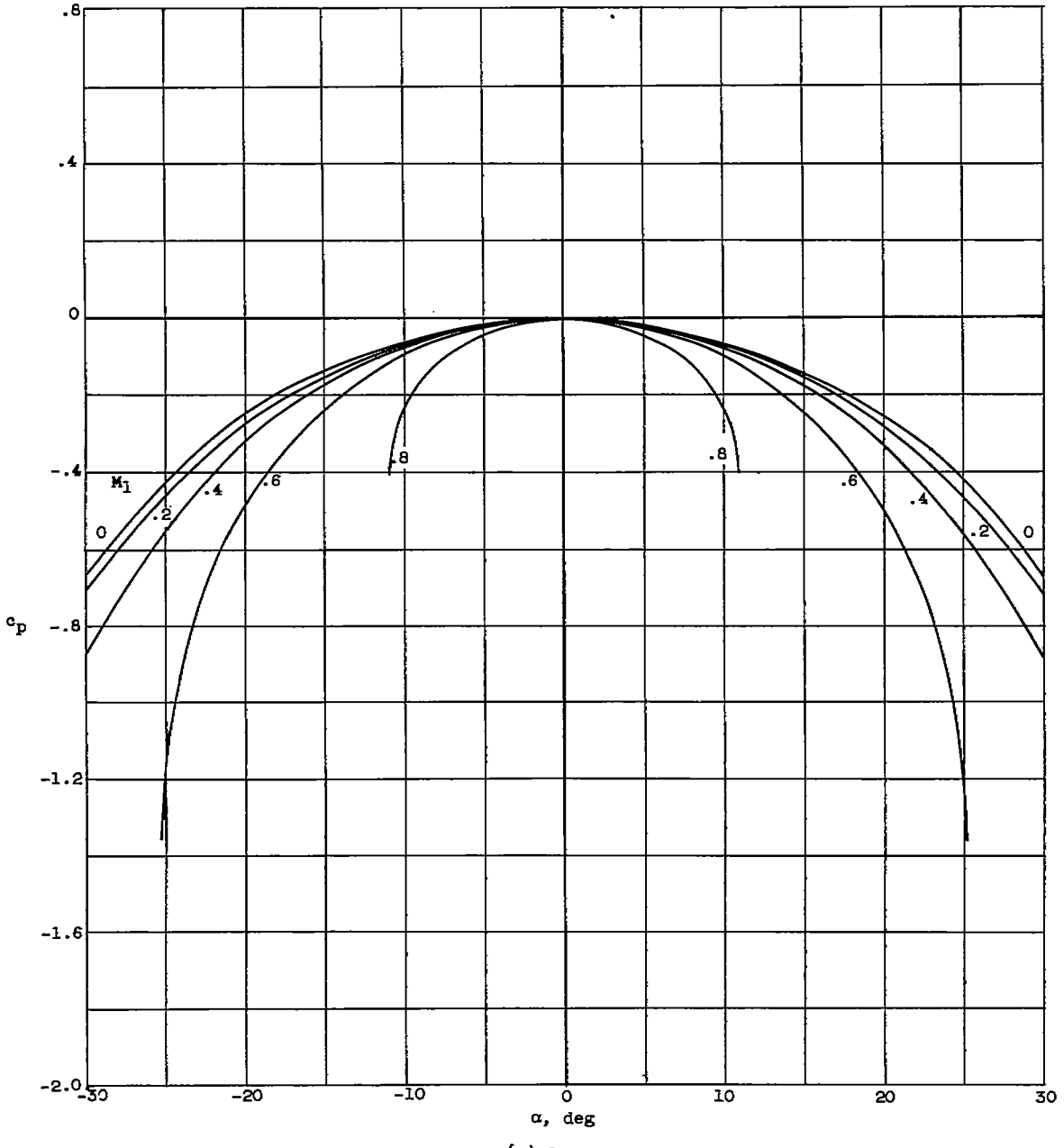

(a) β_1, 0.

Figure 12. - Variation of static-pressure coefficient c_p with angle of attack α for various values of upstream flow angle β_1 and upstream Mach number M_1. Downstream flow deviation angle δ assumed equal to zero.

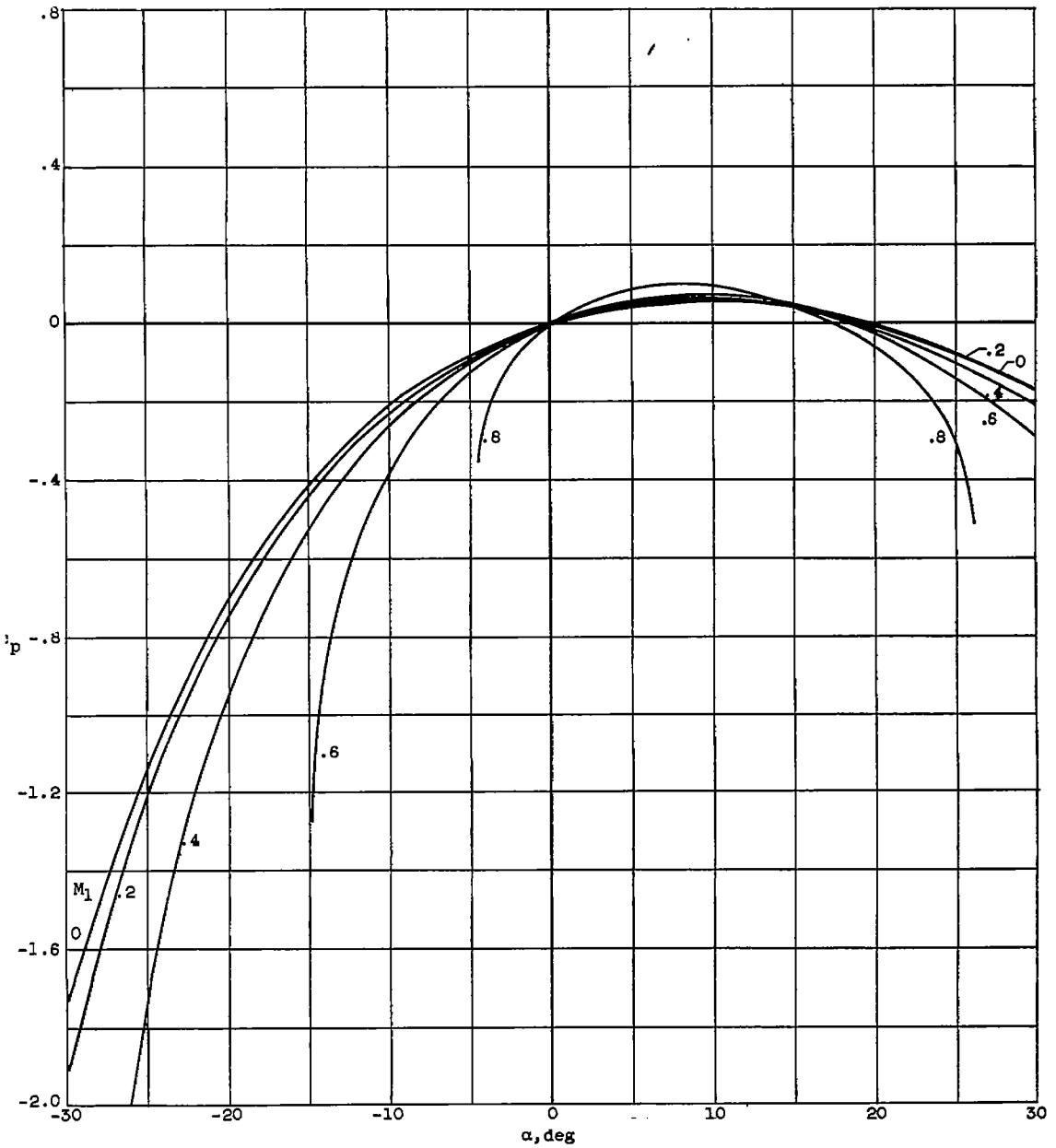

(b) β_1, 20°.

Figure 12. - Continued. Variation of static-pressure coefficient c_p with angle of attack α for various values of upstream flow angle β_1 and upstream Mach number M_1. Downstream flow deviation angle δ assumed equal to zero.

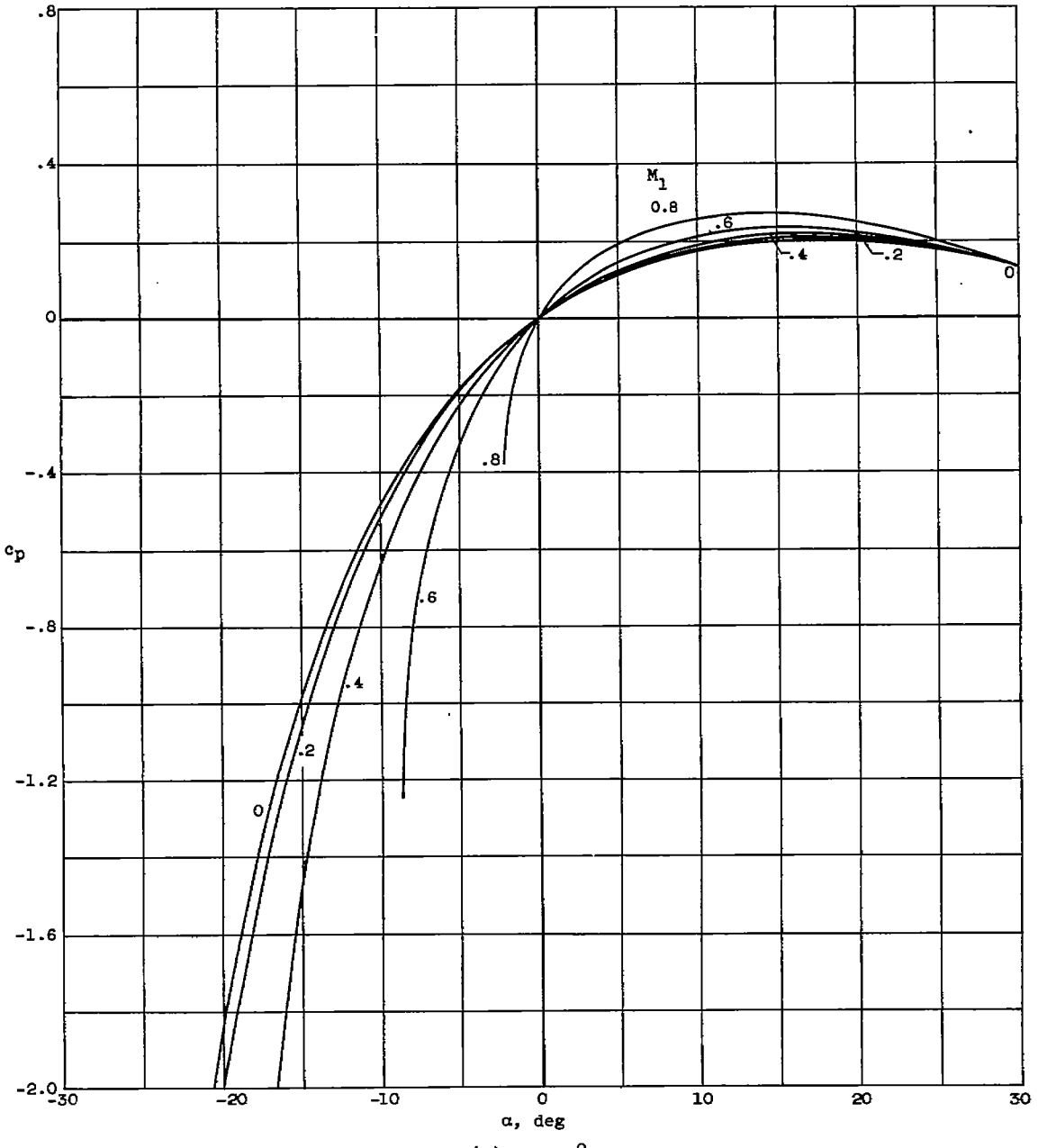

(c) β_1, 40°.

Figure 12. - Continued. Variation of static-pressure coefficient c_p with angle of attack α for various values of upstream flow angle β_1 and upstream Mach number M_1. Downstream flow deviation angle δ assumed equal to zero.

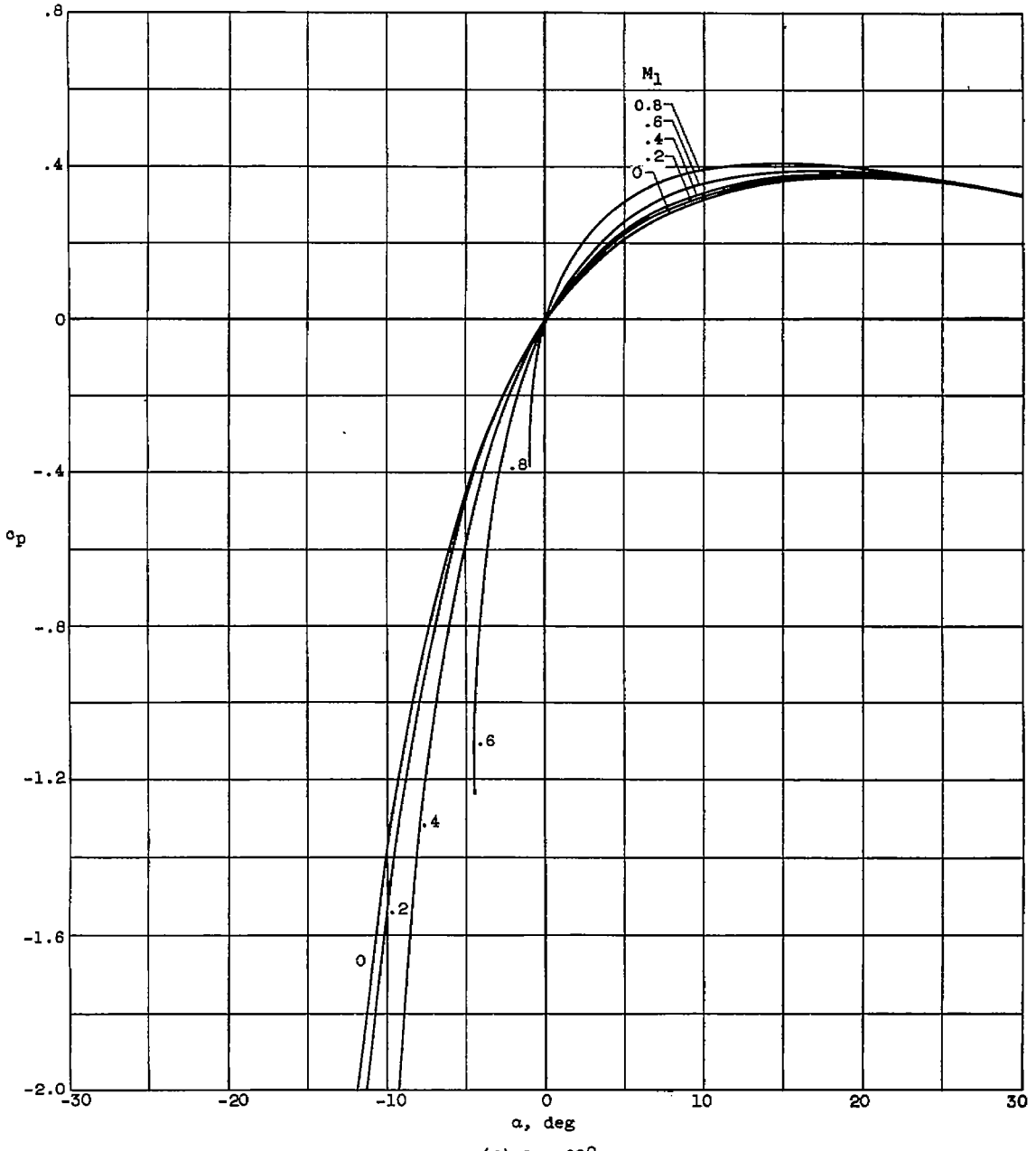

(d) β_1, 60°.

Figure 12. - Continued. Variation of static-pressure coefficient c_p with angle of attack α for various values of upstream flow angle β_1 and upstream Mach number M_1. Downstream flow deviation angle δ assumed equal to zero.

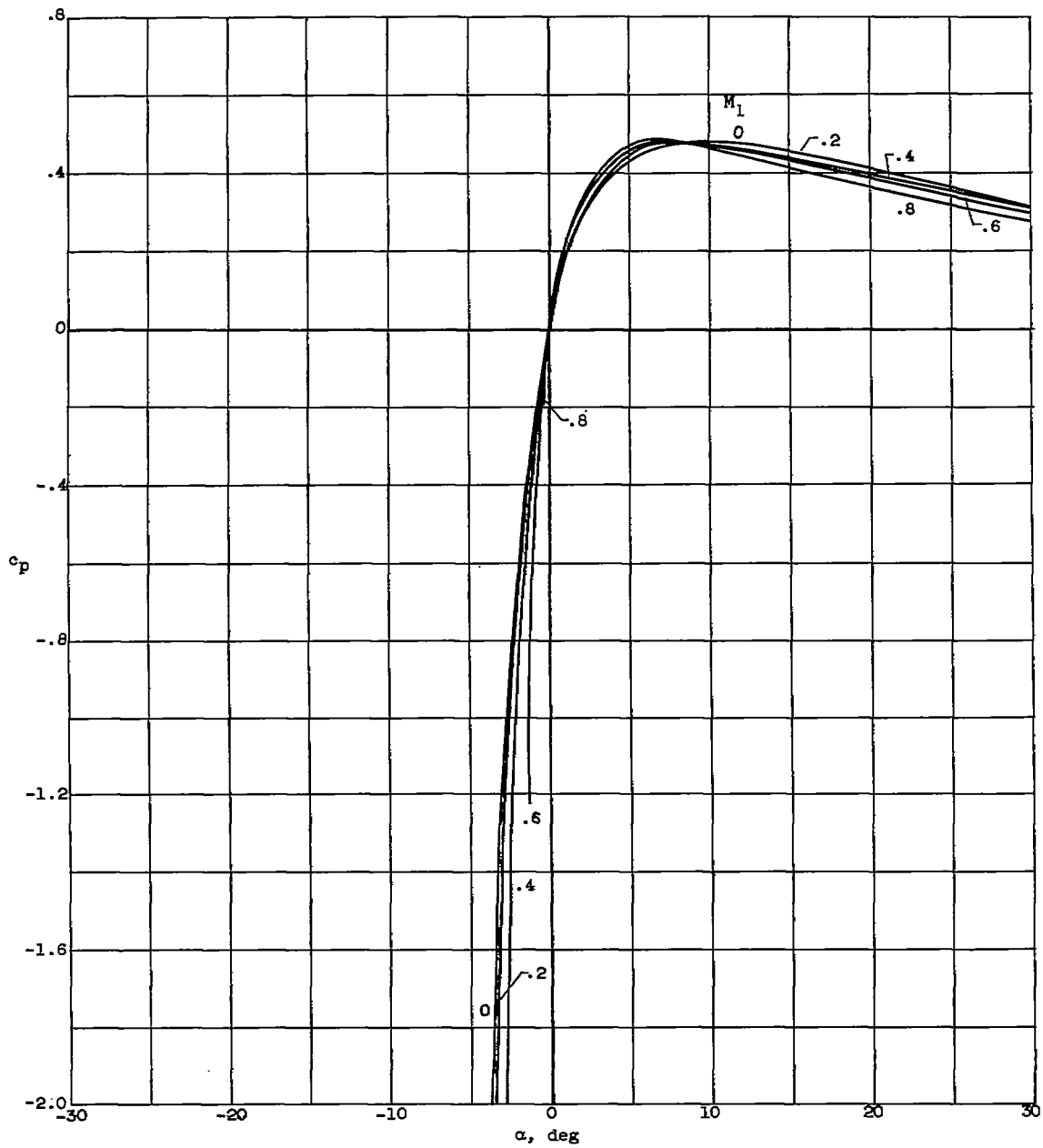

(e) β_1, 80°.

Figure 12. - Concluded. Variation of static-pressure coefficient c_p with angle of attack α for various values of upstream flow angle β_1 and upstream Mach number M_1. Downstream flow deviation angle δ assumed equal to zero.